J. Fluid Mech. (1993), *vol.* 252, *pp.* 667–702

Effects of surface cooling on the spreading of lava flows and domes

By ROSS W. GRIFFITHS[1] AND JONATHAN H. FINK[2]

[1] Research School of Earth Sciences, Australian National University, GPO Box 4, Canberra ACT 2601, Australia

[2] Geology Department, Arizona State University, Tempe, AZ 85287-1404, USA

(Received 14 July 1992 and in revised form 23 December 1992)

Scaling analyses describe the evolution of an extrusion of viscous or plastic fluid in the presence of surface cooling and solidification, under the assumption that the flows consist of two components: an isothermal interior and a surface crust. The 'crust' is a complex thermal and rheological boundary layer which we model using a viscous, plastic or brittle rheology. These models are thought to be relevant to some types of lava flows and address the effects of cooling on their morphology and rate of advance of the flow front. They show that effects of crust strength will dominate over both viscous and yield stresses in the interior when the ratio of crust thickness to flow length exceeds the ratio of effective yield stress of the crust to basal shear stress exerted on the bulk of the flow, a condition that appears likely to be met by many lava flows and small outgrowths on large flows. Similarity solutions are compared with measurements on the spreading of extrusions of wax beneath cold water in the laboratory, where the extruded liquid is viscous but develops a solid crust. Crust strength provides the dominant retarding force for the wax flows in cases where surface solidification occurs rapidly compared with lateral advection. These conditions give flows topped by sheets of solid that buckle or rift apart, or extrusions that enlarge by small bulbous outgrowths (analogous to 'pillows' on submarine lavas and 'toes' on some sub-aerial basalt flows). A comparison of the models with data for the growth of lava domes in the craters of Mount St Helens and Soufrière of St Vincent volcanoes reveals that spreading of those domes was not controlled by stresses in the flow interior. Instead the data are consistent with a balance between gravity and yield stresses in a thin crustal layer over most of the growth period.

1. Introduction

It has long been recognized that the shape and evolution of lava extrusions must be related to the mechanical properties of the magma, its rate of eruption and the volume emplaced (e.g. Walker 1973; Hulme 1974). In the context of the growth of lava domes three idealized mechanical models have been studied in detail: radial flow of an isothermal fluid having uniform Newtonian viscosity (Huppert *et al.* 1982), spreading of an isothermal Bingham fluid (Blake 1990), and inflation of a pressurized dome of fluid encapsulated by a brittle crust (Iverson 1990). An unresolved question has been the role of cooling, with its consequent rheological changes, in governing the flow structure and advance of the flow front. Observations of lava flows reveal that in most cases cooling during the active stages of eruption is confined to a thin surface layer. Cooling leads to a carapace, which is at least partly solid and brittle, on the top surface

of a lava flow. There can also be a cooled basal layer. The flow front advances while cooling is taking place, and the solidified crust deforms in response to the flow.

One observation which may appear trivial at first but which is directly relevant to the role of cooling is that the spreading of lava invariably stops at some time after the vent extrusion ceases. However, in a purely viscous fluid spreading over a horizontal or sloping surface under gravitational forces the strain rate will never vanish (unless surface tension becomes significant or the flow is ponded by underlying topography). Hence it can be concluded that, in the absence of pre-existing topography, a finite yield strength (either in shearing or in tension) is responsible for stopping the motion of lava. The relevant yield strength may be that of the magma at the vent temperature, or it may be a result of cooling of the magma as it loses heat to its new environment. The final extent of a lava flow, or of a small outbreak from the front of a flow, presumably depends on the rates of cooling and spreading of the lava during the effusion period and the time elapsed after effusion ceases and before the extrusion becomes controlled by the strength of some portion of the flow. All of these factors will depend on whether the mechanical control derives from the rheology of the magma at the eruption temperature or of only a relatively cool surface layer.

The role of a finite yield stress for lavas in shear at sub-liquidus temperatures was recognized by Shaw (1969), Hulme (1974) and others, and spreading has been modelled using a uniform, isothermal Bingham material (Blake 1990). The flow in this model can pass from an initial regime of viscous flow into a regime in which there is a static balance between the buoyancy force (resulting from gravity acting on the density difference between lava and the surrounding air or water) and the integrated yield stress. Once in the latter regime the flow stops as soon as the supply of magma ceases. In this case the advance of the flow front will be limited by the erupted volume. That is, the extent of a flow will be 'volume limited' if the forces opposing gravity are predominantly due to the yield strength of the magma at vent temperatures. In contrast, the extent of a flow can be 'cooling limited' if, as envisaged by many previous workers (Shaw & Swanson 1970; Walker 1973; Pinkerton & Sparks 1976; Wilson & Head 1983; Pinkerton 1987), the spreading is halted by an additional strength gained as a result of heat loss from the lava. In both cases the mechanics are, at least in the later stages of emplacement, very different from the dynamics predicted by a viscous gravity current model (Huppert 1982; Huppert *et al.* 1982), in which the front continues to advance indefinitely at a rate determined by a balance between the buoyancy and viscous shear stress.

In contrast to isothermal models, cooling of some portion of the flow and solidification of a crustal layer imply that there is no longer a fixed, well-defined yield strength or viscosity with which to characterize the flow. Instead, it must be acknowledged that for most flows the lava rheology is heterogeneous. For flows having small Reynolds numbers (which imply an absence of turbulent mixing) there is a brittle solid (carapace) covering much of the lava surface, often an accumulation of solid (talus) that has fallen onto the ground at the flow front, and probably a more viscous but not yet solidified layer beneath the surface solid. Even in cases where the solid is extensively fractured or does not form a continuous layer these components support stresses, and the effects of any of them in impeding further advance of the front might potentially be greater than the effects of the basal shear stress on the interior fluid.

One example of the possible role played by the stronger crust is discussed by Iverson (1990) who presented a detailed calculation in which the tensile strength of an outer brittle shell during the growth of a small lava dome is in balance with the sum of the hydrostatic pressure and overpressure. However, this is but one of several possible

dynamical regimes involving the complex surface layer, whose relevant property may instead be a plastic shearing strength or an effective viscosity. Iverson also did not investigate the effects of a time-dependent crust thickness. As another example, the solid carapace and talus apron may determine the apparent viscosity of large andesitic lava domes. A dominant role for the surface layer of one such dome in the crater of La Soufrière is probably responsible for the very large apparent value of viscosity obtained from a comparison of measurements of dome volume and radius with the theory for homogeneous viscous gravity currents (Huppert *et al.* 1982), a comparison which we will show to be inappropriate.

The extent of penetration of cooling into the interior of a lava flow and the role of heat loss in halting a flow front has often been described by a Graetz number, a measure of the length of a flow relative to the length at which the conductive thermal boundary layers would have penetrated through some fraction of the depth of the flow (Pinkerton & Sparks 1976). However, the dynamical consequences of the stronger boundary layers largely remain unpredicted and the critical value of the Graetz number at which a flow will stop advancing remains an empirical one.

A dynamical role for the stiffer crust is also implicit in studies of flow morphology. These have attempted to relate characteristics of the flow structure and surface deformations to the local underlying flow (Fink & Fletcher 1978) or to the vent conditions (Pinkerton 1987; Fink & Griffiths 1990, 1992). In the other direction, the crust imposes a stress on the underlying flow and the morphology reflects the extent to which the crust has slowed, redirected or halted the flow. For example, pillow lavas are produced by irregular short-lived outbreaks of magma from breaks in a strong, rapidly chilled crust, marginal levees of solidified magma have a shearing yield strength great enough to impound the hotter lava, and the folded ('ropy') structure of some Hawaiian (pahoehoe) basalt flows indicates that the crust was thin and ductile and was less able to influence the underlying flow. Flow morphology is thus a potential indicator of the dynamical role played by cooling and solidification in controlling the spreading of a lava flow. Relationships between surface morphology and overall flow conditions were explored by Fink & Griffiths (1990, 1992) (hereinafter referred to as I and II) in a series of laboratory experiments with polyethylene glycol wax. In these experiments wax was injected at temperatures a little above its freezing point through either a small hole (I) or a long narrow slit (II) in the base of a tank of cold water. During its extrusion some wax solidified and formed a crust over the underlying viscous liquid. A sequence of distinctly different flow morphologies was observed as conditions were varied, and each type of structure was identified with counterparts on lava flows.

Here we discuss the dynamics of lava (or wax) flows involving a hot interior enveloped by a cooling, outer boundary layer. For convenience we refer to the outer layer as the 'crust', but this may be some combination of fractured brittle solid, ductile solid and cooled viscous melt. The crust is allowed to thicken in time and its effects are assumed to result from an effective viscosity, shear strength or tensile strength. The interior is allowed to be either viscous or plastic. We consider these two-component flows models to be the next logical step beyond the previous homogeneous viscous and viscoplastic models. They include at one extreme Iverson's (1990) pressurized brittle shell, and at the other Huppert's (1982) isothermal viscous model. Measurements of the evolution of laboratory wax flows are presented, showing the relations between depth, spreading distance and time, along with the dependence of these relations on effusion rate and thermal conditions. The set of morphologic regimes reported previously (I, II) is placed in the context of the dynamical regimes now identified for

those experiments. Finally, the results are compared with data for the growth of two lava domes.

2. Dynamical regimes for a two-component flow

2.1. *The extrusion*

A dynamic model for lava flows which includes the role of surface cooling, but which is still sufficiently simple to be amenable to analytical solutions, is one in which the flow is considered to be made up of two distinct components. When magma issues from a vent its surface is cooled rapidly, forming a relatively strong or viscous 'crust' over the lava surface. Assuming that this rheologically distinct boundary layer is thin compared to the flow depth and is not continually re-engulfed into the interior of the flow (thus excluding very turbulent flows) cooling will be confined to the boundary layer. The temperature and rheology of the bulk of the underlying lava will remain close to that at the vent. Hence we assume a uniform interior (figure 1). Thus only simple flows having a single cooled surface and a largely mobile crust (figure 1) are modelled. These include small segments of lava flows, such as individual 'pillows' of submarine basalts and 'toes' of sub-aerial pahoehoe basalts, as well as large andesite lava domes, rhyolite flows and some extensive basalt flows. The model is not satisfactory for more complex structures, such as compound lava flows (Walker 1972; Kilburn & Lopes 1991) and does not describe flow in lava tubes beneath an immobile crust. Effects of a cooled bottom boundary layer are neglected because conductive heat transfer to the base is relatively slow. Also neglected are any effects of over-running of the cooled crust by the flow front as shown in figure 1.

The interior of the lava flow is modelled as a fluid with a constant Newtonian viscosity or yield stress (the two asymptotic cases for a Bingham fluid). Real lavas will generally have a strain rate-dependent viscosity, and this too could be included in the following similarity solutions by assuming a 'power law' fluid. However, it is appropriate to first explore the implications of the presence of a strong and developing crustal layer using Newtonian and Bingham models for the interior of the flow. The wax used in the laboratory experiments has a constant viscosity at a given temperature for the strain rates achieved. Hence any extrapolation to lavas from wax models will require that the apparent lava viscosity be evaluated for a representative strain rate.

We concentrate on the case of a lava extruded from a point or line source onto a non-slip, horizontal planar surface. (For extrusions onto sloping surfaces the gravitational force is simply modified by the cosine of the angle of inclination from the horizontal, but the flow is no longer symmetric and solutions will be more complicated.) We also let the extruded volume V (or volume per unit length) of lava vary as

$$V = Qt^{\alpha} \quad (\text{or } V = qt^{\alpha}), \tag{1}$$

depending on whether the source is a point (or line) and where t is the time since commencement of the extrusion. In this flexible notation, first suggested by Huppert (1982), the index α may take any value greater than or equal to zero: $\alpha = 0$ denotes spreading of a fixed volume Q (or volume per unit length q), whereas $\alpha = 1$ corresponds to a constant effusion rate Q (or effusion rate per unit length q). In most eruptions the effusion rate decreases with time, placing $\alpha < 1$ (and the dimensions of Q are neither volume or volume per unit time). Others may maintain their flow rate for a period before declining, and some may involve periods of increasing flux, for which α may be greater than one. However, rapid increases generally will not be sustained, so that $\alpha > 2$ is not of interest.

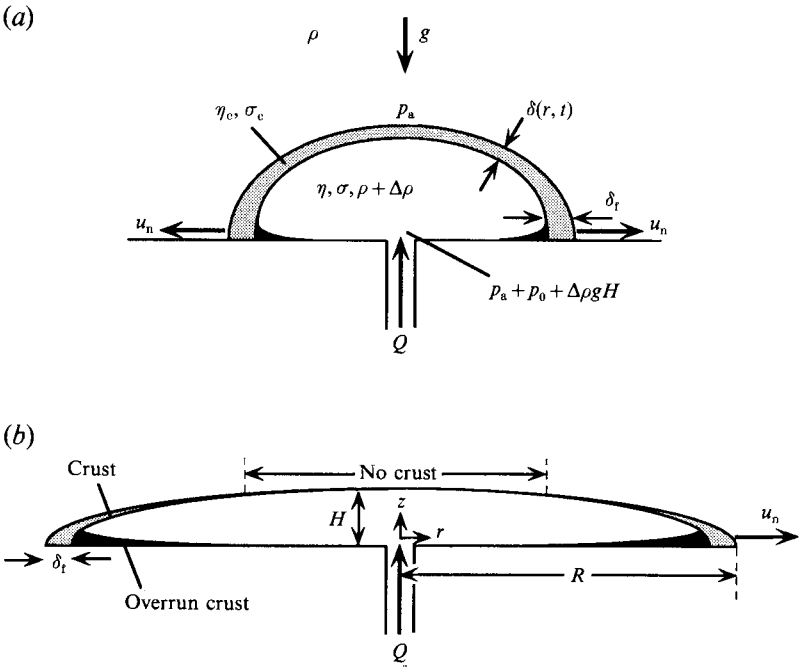

FIGURE 1. Diagrams illustrating the idealized two-component model for lava flows. (*a*) If the effusion rate is small, magma viscosity is large and cooling is rapid, a dome forms with a solid shell over the whole of the flow. (*b*) If the extrusion rate is large and viscosity small, spreading is rapid and solid crust develops only farther from the vent. Variables and assumptions are discussed in the text.

If the point source is assumed to give rise to an approximately axisymmetric flow with radius $R(t)$ and the line source to an approximately two-dimensional spreading with length $L(t)$ normal to the vent, the accumulated volume is given by

$$V = c_1 HR^2 \quad (\text{or } V = c_2 HL), \tag{2}$$

where $H(t)$ is the maximum depth of the flow and c_1, c_2 are factors that take into account the shapes of the depth profiles $h(r)$ and $h(x)$. These shape factors are discussed later.

2.2. *Driving forces*

A number of asymptotic dynamical regimes can be identified, each featuring a simple force balance which can be formulated in terms of the forces integrated over the volume of the flow. The forces available to affect the motion of lava after it emerges from the vent (assuming the rate of extrusion (1) is imposed by external factors) result from inertia, the pressure difference between the vent and the environment, and the stresses associated with deformation of the material. Inertial regimes for extrusions have uniform and constant viscosity have been analysed by Huppert (1982), Didden & Maxworthy (1982) and Lister & Kerr (1989), and may apply to the early stages of some rapid basaltic eruptions. However, for most extrusions of lava, and the wax flows in our experiments, the inertial regime occurs only at very small times after the start of the extrusion. Thus it will not be discussed further.

The pressure difference consists of both the hydrostatic component $\rho g' H$ (where ρ is the density of the lava, $g' = g\Delta\rho/\rho$ is the reduced gravity, $\Delta\rho$ is the density difference between the lava and its environment and g is the acceleration due to gravity) and the overpressure component p_0 (which is simply the total pressure, p, at the vent less the

hydrostatic component and the pressure p_a applied by the environment). These components provide the order-of-magnitude integrated forces (or forces per unit length in the case of a line source) due to buoyancy

$$F_B \sim \rho g' H^2 R \quad (\text{or } \rho g' H^2), \tag{3}$$

and overpressure

$$F_P \sim p_0 R^2 \quad (\text{or } p_0 L). \tag{4}$$

When buoyancy is the dominant driving force the horizontal scale of the extrusion will tend to grow more rapidly than the depth H. However, in the limit of $F_P \gg F_B$, body forces are negligible and the extrusion must take on an approximately spherical (or cylindrical) shape, distorted only by effects of the rigid non-slip base on which the vent lies and, possibly, by asymmetric outflows from fractures of the surface. Relations (1)–(4) are not affected by the thermal and rheological structure of an extrusion.

2.3. *Retarding forces from the interior*

Stresses retarding the flow may arise from the rate of strain $\partial u/\partial r$, shear $\partial u/\partial z$ (resulting from the non-slip boundary condition on the base, where u is the radial velocity in the horizontal and z is the distance from the base), shear strength and tensile strength. In flows having uniform Newtonian viscosity (η) the forces F_τ resulting from shear stress $\eta \partial u/\partial z$ acting over the basal area of the flow (as in Huppert 1982) and those due to internal viscous stress $\eta \partial u/\partial r$ in a growing dome both scale as:

$$F_\tau \sim \eta \dot{\epsilon} R^2 \quad (\text{or } \eta \dot{\epsilon} L), \tag{5}$$

where $\dot{\epsilon}$ is the strain rate.

The strain rate in (5) can be replaced by $\dot{\epsilon} \sim U/R$ for radial shortening of fluid elements, and by $\dot{\epsilon} \sim U/H$ for basal shear stress. In both cases U is the speed of advance of the flow front and scales as $U = \mathrm{d}R/\mathrm{d}t \sim R/t$. The two contributions to the viscous force become $F_\tau \sim \eta R^2/t$ and $F_\tau \sim \eta R^3/Ht$, respectively. Hence the two will be comparable at small times, when the radius and height are comparable, whereas basal shear stress comes to dominate as the flow becomes broader ($R \gg H$). The former regime may be relevant to individual outgrowths such as those that form a single submarine pillow or a small lobe of a lava dome, whereas the latter case will apply to most stages of the development of lava flows.

If the flow interior has a yield stress (σ), the integral of this over the basal area of the flow provides a retarding force

$$F_\sigma \sim \sigma R^2 \quad (\text{or } \sigma L). \tag{6}$$

Blake (1990), following earlier work by Hulme (1974), modelled the extruded material as a Bingham fluid and showed that, under suitable conditions, there will be a static balance in which the buoyancy force (3) is equated to the shear strength (6). In this Bingham model the retarding force changes from that given by (5), which applies when $\sigma \ll \eta \dot{\epsilon}$ (i.e. $t \ll \eta R/\sigma H$), to that given by (6), when $\sigma \gg \eta \dot{\epsilon}$. Note that if $H \sim R$ (as occurs when buoyancy effects are negligible), this transition occurs at a time $t \sim \eta/\sigma$.

2.4. *Retarding forces from the crust*

If surface cooling leads to a thin upper layer that is more viscous or stronger than the interior of the flow, the advance of the flow front and the flow depth are potentially influenced by stresses required to deform this crust as well as by the interior stresses. Depending on flow conditions the surface solid on a lava flow can form a continuous ductile sheet over some of the lava surface, can be torn apart into separated fragments,

or can form a dense layer of fractured brittle blocks. In general, the crust will consist of deformed or fractured solid, as well as some intervening melt that has upwelled between segments of solid (Crisp & Baloga 1990) and some underlying cooled melt. In some cases advection of crust during spreading can lead to an accumulation of deformed crust at the flow front. Thus, the effective mechanical properties of the crust are uncertain. An abundance of solid on the surface does not necessarily imply that this rheological boundary layer behaves as a brittle crust on the scale of the flow and it is probable that a crust of fragmented brittle material, with pieces of solid moving relative to each other, is more closely described by a viscous or plastic rheology. The effective rheology of the crustal layer on the laboratory wax flows too, is unknown. Under some conditions the wax crust shows evidence of ductile deformation, while under other conditions it appears to behave as a brittle solid. Neither represents the effective behaviour of the whole surface layer under all conditions.

We consider the three simplest possibilities for the crust: an effective Newtonian viscosity (which is potentially much greater than the viscosity of the interior fluid), a plastic yield stress (which again may be much greater than the yield strength of the interior magma) or a tensile strength. Surface temperature is one of the most important determinants of rheology. However, this falls far below the solidification temperature and approaches the ambient temperature over times shorter than the duration of most eruptions (falling to within 300 K of ambient in a minute under water and a day under air, from the calculations of Griffiths & Fink 1992*a*, *b*). Hence we neglect variations of crust viscosity or strength with time during spreading in each dynamical regime. Although this assumption precludes changes in effective rheology due to continuing decrease of surface temperature, it does not prevent changes due to thickening of the crust.

For flows which are broad and shallow, advancing by either a bulk motion of the flow front or intermittent new outbreaks from the front, most of the crustal resistance will derive from the flow front. There the crust must undergo the greatest deformation to allow flow or fracture. For flows which are as deep as they are long, on the other hand, the whole of the surface can be seen as the flow front. If the crust has an effective viscosity $\eta_c (\eta_c \gg \eta)$, the additional contribution $F_{\tau c}$ to the retarding force ((5) or (6)) is

$$F_{\tau c} \sim \eta_c \dot{\epsilon} R \delta_f \quad (\text{or } \eta_c \dot{\epsilon} \delta_f), \tag{7}$$

where δ_f is the crust thickness near the flow front (figure 1). Alternatively, if the crust is plastic and has an effective shearing strength σ_c, the additional retarding force has a magnitude

$$F_{\sigma c} \sim \sigma_c R \delta_f \quad (\text{or } \sigma_c \delta_f). \tag{8}$$

The use of a shear strength in (8) may be appropriate if motion of the lava is driven by buoyancy and involves deformation of the crust primarily near the flow front by shearing or rolling over. However, some flows may also be influenced by the tensile strength of a brittle crust in tension, as is the case during inflation of a small lava dome analysed by Iverson (1990) and Denlinger (1990). Fracturing of a brittle crust in tension is particularly likely when overpressure is comparable to, or dominates over, the buoyancy force, because the resulting equant inflation leads to smaller shearing stresses and the whole of the surface comes into tension. In such cases a yield stress in tension (γ_c) may be more appropriate in (8) than the shear strength σ_c, but the form of the relation is unchanged.

We approximate the crust thickness near the flow front in (7) and (8) as proportional to the thickness of a conductive thermal boundary layer which develops as the flow

advances: following an element of the crust as it is advected we write $\delta_f \sim (\kappa t)^{\frac{1}{2}}$, where t is the time since the eruption commenced and κ is the thermal diffusivity. This $t^{\frac{1}{2}}$-dependence of effective crust thickness assumes that the thermal and rheological boundary layers thicken by one-dimensional conduction of heat to the flow surface. For very flat spreading flows with rapid effusion and slow solidification this thickening with time occurs as the surface layer is advected horizontally away from the vent, and during endogenous inflation of small domes or pillows it will occur more or less uniformly over the dome surface (figure 1). Thus the assumed dependence is expected to be a reasonable approximation for the thickness of the thermal boundary layer, and also for the depth of the solidification front at times much greater than those required for the initial onset of freezing (Griffiths & Fink 1992*a*). It does not rely on assumptions about the presence or absence of effects of release of latent heat of fusion since the same time-dependence of crust thickness is given by solution of the one-dimensional Stefan problem.

The $t^{\frac{1}{2}}$-dependence neglects any additional increase or decrease of the crust thickness resulting from surface compression or extension, respectively. Compression in the direction of motion occurs over much of the surface behind the flow front, and leads to folding of the crust in cases where the crust is thin or weak (Fink & Fletcher 1978; I). Extension in the direction of motion tends to occur directly over the vent (or where underlying slope increases, but this case is not considered here). If the flow is diverging, as in radial spreading, extension normal to the motion is more widespread (I). However, in radial spreading the changes in thickness of an element of the thermal boundary layer owing to compression and extension in the plane of the surface tend to offset each other. In cases with strong crust the effects of localized extension, where fragments of solid are pulled apart intermittently exposing small areas of melt, can be neglected since only an average crust thickness is required in the present model. The $t^{\frac{1}{2}}$ evolution does, however, assume that cold boundary-layer material is not carried away from the surface by internal motions. This requires only that the stiffness of the cold surface layer acts to maintain stability against convective subduction and turbulent entrainment. Yet another situation arises if the interior fluid is channellized and flows beneath an immobile carapace to emerge at the flow front, as in lava tubes. The melt then loses little heat in transit to the front, where the crust may be thinnest. In this case the analysis to follow applies only to the growth of the extrusions ('toes', 'pillows' or 'lobes') at the flow front.

2.5. *Similarity solutions*

Either the buoyancy force (3) or pressure force (4) can be equated to any one of the forces, (5)–(8), arising from the material strength or viscosity. The consequent time-dependence of radius and depth can be found using the volume (1) and geometric relation (2), along with scaling discussed above for the strain rate and crust thickness. Results for the eight dynamical regimes, assuming the shape factor in (2) is constant with time in each regime, are summarized in table 1. These self-similar solutions are known to exist for the isothermal viscous and Bingham gravity currents (denoted by BNI and BPI, respectively, where the initials are explained in table 1). However, for crust viscosity or strength in balance with buoyancy our assumption of constant shape factors is expected to be only an approximation.

There are a number of differences among the predicted behaviours in table 1 which are of interest, particularly as potential discriminators in placing a flow in a dynamical regime according to the evolution of radius and height. For example, if $\alpha = 1$ (constant effusion rate), regimes BNI (buoyancy–Newtonian interior) and BCS (buoyancy–crust

Point source

	Regime	Driving force	Retarding force	$R(t)$	$H(t)$	$H(R)$
BNI	Buoyancy *vs.* Newtonian shear stress on flow interior	$\rho g' H^2 R$	$\eta \dot{\epsilon} R^2$	$\left[\frac{\rho g'}{\eta} Q^3 t^{3\alpha+1}\right]^{\frac{1}{8}}$	$\left[\frac{\eta Q}{\rho g'} t^{(\alpha-1)}\right]^{\frac{1}{4}}$	$\left[\left(\frac{\eta}{\rho g'}\right)^{\alpha} Q R^{2\alpha-2}\right]^{1/(3\alpha+1)}$
BPI	Buoyancy *vs.* yield stress in flow interior	$\rho g' H^2 R$	σR^2	$\left[\frac{\rho g'}{\sigma} Q^2 t^{2\alpha}\right]^{\frac{1}{5}}$	$\left(\frac{\sigma}{\rho g'}\right)^{\frac{2}{5}} Q^{\frac{1}{5}} t^{\frac{1}{5}\alpha}$	$\left(\frac{\sigma}{\rho g'} R\right)^{\frac{1}{2}}$
BNC	Buoyancy *vs.* Newtonian shear stress in crust	$\rho g' H^2 R$	$\eta_c \dot{\epsilon} R \delta_t$	$\left[\frac{\rho g'}{\eta_c} \kappa^{-\frac{1}{2}} Q^3 t^{\frac{1}{2}(6\alpha+1)}\right]^{\frac{1}{7}}$	$\left(\frac{\eta_c}{\rho g'}\right)^{\frac{2}{7}} (\kappa Q)^{\frac{1}{7}} t^{\frac{1}{7}(\alpha-1)}$	$\left[\left(\frac{\eta_c}{\rho g'}\right)^{2\alpha} \kappa^{\alpha} Q R^{2\alpha-2}\right]^{1/(6\alpha+1)}$
BCS	Buoyancy *vs.* yield stress in crust	$\rho g' H^2 R$	$\sigma_c R \delta_t$	$\left[\frac{\rho g'}{\sigma_c} \kappa^{-\frac{1}{2}} Q^2 t^{\frac{1}{2}(4\alpha-1)}\right]^{\frac{1}{4}}$	$\left(\frac{\sigma_c}{\rho g'}\right)^{\frac{1}{2}} (\kappa t)^{\frac{1}{4}}$	$\left[\left(\frac{\sigma_c}{\rho g'}\right)^{2\alpha} \kappa^{\alpha} Q^{-1} R^2\right]^{1/(4\alpha-1)}$
PCS	Overpressure dominant	pR^2	Any of the above	$(Qt^{\alpha})^{\frac{1}{3}}$	$(Qt^{\alpha})^{\frac{1}{3}}$	R

Line source

	Regime	Driving force	Retarding force	$L(t)$	$H(t)$	$H(L)$
BNI	Buoyancy *vs.* Newtonian shear stress on flow interior	$\rho g' H^2$	$\eta \dot{\epsilon} L$	$\left[\frac{\rho g'}{\eta} q^3 t^{3\alpha+1}\right]^{\frac{1}{5}}$	$\left[\frac{\eta}{\rho g'} q^2 t^{2\alpha-1}\right]^{\frac{1}{5}}$	$\left[\left(\frac{\eta}{\rho g'}\right)^{\frac{\alpha+2}{5}} q L^{2\alpha-1}\right]^{1/(3\alpha+1)}$
BPI	Buoyancy *vs.* yield stress in flow interior	$\rho g' H^2$	σL	$\left[\frac{\rho g'}{\sigma} q^2 t^{2\alpha}\right]^{\frac{1}{3}}$	$\left[\frac{\sigma}{\rho g'} q t^{\alpha}\right]^{\frac{1}{3}}$	$\left(\frac{\sigma}{\rho g'} L\right)^{\frac{1}{2}}$
BNC	Buoyancy *vs.* Newtonian shear stress in crust	$\rho g' H^2$	$\eta_c \dot{\epsilon} \delta_t$	$\left[\frac{\rho g'}{\eta_c} \kappa^{-\frac{1}{2}} q^3 t^{\frac{1}{2}(6\alpha+1)}\right]^{\frac{1}{4}}$	$\left[\frac{\eta_c}{\rho g'} \kappa^{\frac{1}{2}} q t^{\frac{1}{2}(2\alpha-1)}\right]^{\frac{1}{4}}$	$\left[\left(\frac{\eta_c}{\rho g'}\right)^{2\alpha} \kappa^{\alpha} q L^{2\alpha-1}\right]^{1/(6\alpha+1)}$
BCS	Buoyancy *vs.* yield stress in crust	$\rho g' H^2$	$\sigma_c \delta_t$	$\left(\frac{\rho g'}{\sigma_c}\right)^{\frac{1}{2}} \kappa^{-\frac{1}{4}} q t^{\alpha-\frac{1}{4}}$	$\left(\frac{\sigma_c}{\rho g'}\right)^{\frac{1}{2}} (\kappa t)^{\frac{1}{4}}$	$\left[\left(\frac{\sigma_c}{\rho g'}\right)^{2\alpha} \kappa^{\alpha} q^{-1} L\right]^{1/(4\alpha+1)}$
PCS	Overpressure dominant	pL	Any of the above	$(qt^{\alpha})^{\frac{1}{2}}$	$(qt^{\alpha})^{\frac{1}{2}}$	L

TABLE 1. The flow behaviour predicted for the various dynamical regimes, for point and line sources. The results shown are derived simply by equating the integrated forces and imposing conservation of mass. Regimes involving an effective yield strength of the crust are written in terms of σ_c, the yield stress in shearing flows, but the same scaling applies if a yield stress in tension is relevant, and we do not wish to distinguish between the two. The first regime (BNI) was discussed by Huppert (1982), the second (BPI) by Blake (1990) and the last (PCS) is the overpressure driven limit of the brittle shell model of Iverson (1990). The last three regimes assume a two-component flow consisting of an isothermal interior and a relatively thin, rheologically distinct surface layer.

strength) for point sources are not well distinguished by the dependence of radius on time; they are better differentiated by the depth, since H should be constant for homogeneous buoyancy–viscous flow from a point source, whereas $H \sim t^{\frac{1}{4}}$ and $H \sim R^{\frac{2}{3}}$ are predicted for flow with a strong crust. Predictions for $H(R)$ are useful, in addition to those for $H(t)$ and $R(t)$, because in some cases the power laws they give are more significantly different when compared with the uncertainties in data. Plots of $H(R)$ also give a direct indication of the aspect ratio of an extrusion.

Another useful result in table 1 is that the relation between extrusion depth and radius, which is of the form

$$H \sim \beta R^{\lambda} \tag{9}$$

(or $H \sim \beta L^{\lambda}$ for line sources), involves not only the exponent λ (discussed above) but also the coefficient β, where β depends on the effusion rate parameter Q (or q) in different ways for different dynamical regimes: for regime BNI $\beta \sim Q^{\frac{1}{4}}$ (or $\beta \sim q^{\frac{1}{4}}$), whereas for regime BCS $\beta \sim Q^{-\frac{1}{5}}$ (or $\beta \sim q^{-\frac{1}{5}}$). Thus for buoyancy-driven flows larger effusion rates give greater extrusion depths (at a given flow extent) if the flow is viscous, whereas larger effusion rates give smaller depths if the flow is controlled by strong crust that develops with time. Alternatively, if the primary balance is between overpressure and stresses in the crust, the depth is directly proportional to radius or length, and independent of flow rate.

3. Regime transitions

In order to determine which of the above regimes is likely to occur, and whether transitions from one regime to another are expected, we consider the relative magnitudes of the forces as functions of time during an extrusion. It is necessary first to decide which of (5–8) is the dominant retarding force under given conditions. For brevity, we will be explicit only about radial flow from a point source.

3.1. *Transitions from viscous to plastic homogeneous flow*

The viscous stresses (5) in an homogeneous extrusion are dominant over the yield stress (6) when $\eta\dot{\epsilon}/\sigma \gg 1$. Assuming $R/H \geqslant 1$ this holds when $t \ll (\eta/\sigma)(R/H)$. Thus, if R/H increases with time raised to a power less than one, the extrusion can pass from an initially viscous flow to one controlled by yield strength (Blake 1990). This will be the case for all realistic values of the volume exponent α since a homogeneous viscous flow (case BNI in table 1) has an aspect ratio which evolves as $R/H \sim t^{(\alpha+3)/8}$, where the power is less than one for $\alpha < 5$. For $\alpha < 5$ the depth at transition to plastic flow is $H \sim Q^{\frac{1}{3}}(\eta/\sigma)^{\frac{1}{3}\alpha}$.

3.2. *Dominance of interior versus crustal stresses*

In the presence of cooling both the viscosity and yield strength of a surface layer will be greater than those of the hotter fluid in the interior of a lava flow. From (5)–(8) the crust provides a greater retarding stress than does the interior when

$$\tau_c/\tau > R/\delta_f, \tag{10}$$

where each of the shear stresses may be determined by either the effective viscosities or the yield stresses. Thus, for example, a lava dome of radius 10^3 m having a cooled layer 10 m thick is controlled by shear stresses within the crust if $\eta_c \gg 10^2\eta$ or $\sigma_c \gg 10^2\sigma$. Similarly, a basalt pillow 1 m in radius will be controlled by stresses in a 1 mm thick glassy skin if $\sigma_c \gg 10^3\dot{\epsilon}\eta$. (Cooling calculations indicate that 2 mm of glass will form on submarine extrusions after 10 s of exposure (Griffiths & Fink 1992*b*).) For a pillow

which grows to 1 m radius in 10 s (with $\eta \sim 10^2$ Pa s) crust control requires a strength $\sigma_c \gg 10^4$ Pa (near water temperature), an inequality that is likely to be achieved since shear strengths of order 10^4 Pa were measured for laboratory samples of basalt at temperatures around 1100 °C (McBirney & Murase 1984). In both of these examples the increase in viscosity or strength required to give the crust control over the flow is small compared with the actual increases expected on cooling and solidification of lava (e.g. Shaw 1969; Fink & Fletcher 1978). It is possible that even highly fractured crust and a cooled but not fully solidified thermal boundary layer lead to crustal control.

The dynamical significance of the crust for some flows will vary with time. For example, if an extrusion commences with overpressure providing the dominant driving force at small times (as predicted below) then $R \sim H \sim t^{\frac{1}{5}\alpha}$ (for radial spreading with overpressure balancing crust strength, case PCS, table 1), which gives $R/\delta_f \sim t^{(\frac{1}{5}\alpha - \frac{1}{2})}$. From (10) the relative role of crustal stresses therefore increases with time for values of $\alpha < \frac{3}{2}$. Thus, if such an 'overpressurized' flow is not initially dominated by crustal stresses, it can undergo a transition to a regime that is. Alternatively, if the flow is driven by buoyancy, and initially the dominant retarding force is the basal shear stress on the whole of the flow, then $R \sim t^{\frac{1}{8}(3\alpha+1)}$ or $R \sim t^{\frac{2}{5}\alpha}$ for viscous or plastic flow (cases BNI and BPI), respectively. In these cases the role of crust increases with time for $\alpha < 1$ (viscous interior) or $\alpha < \frac{5}{4}$ (plastic interior), again leading to the possibility of a transition to a new regime dominated by the crust. For example, if an extrusion commences as a uniform viscous flow (BNI) but the solidifying crust is characterized by a plastic or brittle yield stress instead of a viscosity, the ratio of forces due to crust strength and interior viscosity evolves as $\sigma_c \delta_f R/\eta \dot{\epsilon} R^2 \sim t^{\frac{1}{6}(9-2\alpha)}$. Hence the crust strength eventually becomes dominant for all $\alpha < 4.5$, which includes all realistic conditions. Transition to crust control occurs at a time

$$t_c \sim (\eta Q^{\frac{1}{3}}/\sigma_c \kappa^{\frac{1}{2}})^{6/(9-2\alpha)}. \tag{11}$$

The relative roles of viscosity and yield strength in the crust depend on the strain rate: the strength is dominant if $\sigma_c/\eta_c \gg \dot{\epsilon}$. Using $\dot{\epsilon} \sim R/Ht$ and assuming an initially viscous crust (case BNC) the strain rate decreases with time if $\alpha < 2.75$. Therefore (assuming constant values of the effective viscosity and yield stress) the decreasing strain rate causes the crust strength to become dominant over the viscosity.

All of the above results for radial spreading from a point source indicate that many flows eventually become controlled by the effective yield stress in the cooled surface layer. Basal shear stress acting on the bulk of the flow, as envisaged by Huppert (1982), Huppert *et al.* (1982) and Blake (1990), is predicted to be effective in only an early phase of spreading, or not at all. A similar conclusion can be drawn for buoyancy-driven spreading from line sources. In that case the relative role of crustal yield stress (compared with shear stress throughout the interior of the flow) increases with time for a purely viscous interior and crust if $\alpha < \frac{2}{3}$, and for a plastic interior and crust if $\alpha < \frac{3}{4}$. In these cases, where the flow is constrained to be wholly viscous or wholly plastic, a constant effusion rate ($\alpha = 1$) from a line source can lead to the inverse transition, from 'crustal' or 'interior' control. On the other hand, if the line source flow is initially viscous but the crust is plastic or brittle, the transition to control by crust strength is expected for $\alpha < 3$, with transition occurring at a time (corresponding to (11) for a point source)

$$t_c \sim (\eta q^{\frac{1}{2}}/\sigma_c \kappa^{\frac{1}{2}})^{2/(3-\alpha)}. \tag{12}$$

Another useful result is that an extrusion from a line source initially characterized by a balance between overpressure and crust strength (PCS) will continue to be controlled by the crust indefinitely if $\alpha \leqslant 1$.

The above conclusions are based on the assumptions that the crust thickness increases as the square root of time and the viscosity or strength of the surface layer is constant. On the other hand, if the crust thickness were constant, there would generally be a transition from a crust-controlled flow regime to a regime dominated by basal shear stress on the flow interior. However, a more likely alternative is that the effective surface viscosity or strength increases with time in some cases as a result of a decreasing surface temperature or a possible dependence of crust rheology on crust thickness. The tendency toward crust control would then be enhanced. Furthermore, observations reveal that solidification does not occur on the surface within a distance from the vent given by the lateral spreading velocity multiplied by the time for the contact temperature to reach the solidification temperature (I; II; Griffiths & Fink 1992*a*, *b*). Our wax experiments showed that solid formed over the vent only under conditions giving rapid solidification relative to advection, and crust did not appear at the flow front until the late stages of runs having rapid relative spreading rates. The decrease in surface temperature leading to onset of solidification is therefore an additional factor which may lead to transitions between dynamical regimes in flows with rapid effusion and spreading rates: an early stage controlled by a homogeneous viscosity or by the viscosity in a cooled surface layer, followed by a regime controlled by a finite yield stress of the surface layer after onset of solidification.

3.3. *Buoyancy versus overpressure*

In order to determine whether overpressure or buoyancy provides the dominant driving force we consider the beginning of an extrusion and the minimum possible resistance to flow. This minimum resistance derives from the strain rate

$$\dot{\epsilon} \sim \partial u/\partial r \sim U/H$$

which always occurs, even though the resulting stress may be overshadowed by crustal stresses. The total pressure p at the vent required to produce this strain rate can be found by equating the viscous force to the total pressure force: for a point source

$$pR^2 \sim \eta \dot{\epsilon} R^2,$$

which gives

$$p \sim \eta t^{-1}.$$

Thus, for a prescribed effusion rate of the form (1) and a simple viscous flow with no crust, the pressure decreases with time. However, the hydrostatic component of this pressure begins at zero and increases as the extrusion enlarges. For $\alpha > 0$ and $R \sim H \sim (Qt^{\alpha})^{\frac{1}{3}}$ the ratio of the minimum vent pressure force to the buoyancy force is

$$pR^2/\rho g' H^2 R \sim (\eta/\rho g')\, Q^{-\frac{1}{3}} t^{-(1+\frac{1}{3}\alpha)}.$$

Hence the buoyancy force is initially small but increases with time and eventually becomes dominant. The transition from overpressure to buoyancy-driven flow in this case occurs at a time t^*, where

$$t^* \sim (\eta/\rho g' Q^{\frac{1}{3}})^{3/(3+\alpha)}. \tag{13}$$

The time t^* is closely related to the timescale $t_0 = (\eta/\rho g' Q^{\frac{1}{3}})^{\frac{3}{4}\alpha}$, which is that required for the depth of the extrusion to reach $H_0 = (Q\eta/\rho g')^{\frac{1}{3}}$, the depth of an homogeneous viscous gravity current driven by buoyancy (Huppert 1982). For a line source we again find $p \sim t^{-1}$ at small times, the transition to buoyancy-driven flow for $\alpha > 0$ occurs at

Dominant retarding stress	Overpressure at small times	Ratio overpressure to buoyancy	Transition time t^*
		Point source	
Uniform interior viscosity	ηt^{-1}	$(t/t^*)^{-(1+\frac{1}{3}\alpha)}$	$\left(\frac{\eta}{\rho g' Q^{\frac{1}{3}}}\right)^{3/(3+\alpha)}$
Uniform interior yield stress	σ	$(t/t^*)^{-\frac{1}{3}\alpha}$	$\left(\frac{\sigma}{\rho g' Q^{\frac{1}{3}}}\right)^{3/\alpha}$
Crust viscosity	$\eta_c \kappa^{\frac{1}{2}} Q^{-\frac{1}{3}} t^{-\frac{1}{3}(\alpha+\frac{3}{2})}$	$(t/t^*)^{-\frac{2}{3}(\alpha+\frac{3}{4})}$	$\left(\frac{\eta_c \kappa^{\frac{1}{2}}}{\rho g' Q^{\frac{2}{3}}}\right)^{6/(4\alpha+3)}$
Crust strength ($\alpha > \frac{3}{4}$)	$\sigma_c \kappa^{\frac{1}{2}} Q^{-\frac{1}{3}} t^{-\frac{1}{3}(\alpha-\frac{3}{2})}$	$(t/t^*)^{-\frac{2}{3}(\alpha-\frac{3}{4})}$	$\left(\frac{\sigma_c \kappa^{\frac{1}{2}}}{\rho g' Q^{\frac{2}{3}}}\right)^{6/(4\alpha-3)}$
		Line source	
Uniform interior viscosity	ηt^{-1}	$(t/t^*)^{-(1+\frac{1}{2}\alpha)}$	$\left(\frac{\eta}{\rho g' q^{\frac{1}{2}}}\right)^{2/(2+\alpha)}$
Uniform interior yield stress	σ	$(t/t^*)^{-\frac{1}{2}\alpha}$	$\left(\frac{\sigma}{\rho g' q^{\frac{1}{2}}}\right)^{2/\alpha}$
Crust viscosity	$\eta_c \kappa^{\frac{1}{2}} q^{-\frac{1}{2}} t^{-\frac{1}{2}(\alpha+1)}$	$(t/t^*)^{-(\alpha+\frac{1}{2})}$	$\left(\frac{\eta_c \kappa^{\frac{1}{2}}}{\rho g' q}\right)^{2/(2\alpha+1)}$
Crust strength ($\alpha > \frac{1}{2}$)	$\sigma_c \kappa^{\frac{1}{2}} q^{-\frac{1}{2}} t^{-\frac{1}{2}(\alpha-1)}$	$(t/t^*)^{-(\alpha-\frac{1}{2})}$	$\left(\frac{\sigma_c \kappa^{\frac{1}{2}}}{\rho g' q}\right)^{2/(2\alpha-1)}$

TABLE 2. The evolution of flows initially dominated by overpressure. The ratio of overpressure to buoyancy forces generally decreases with time, leading to a transition at time t^* from overpressure dominance to a buoyancy-driven flow regime. The transition time depends on the source of the retarding stress. No transition occurs if the retarding stress is due to the tensile strength of the crust and the volume exponent $\alpha < \frac{3}{4}$ (point source) or $\alpha < \frac{1}{2}$ (line source). Thus slowly extruded lava domes having strong crusts, and for which effusion rates generally pass through a maximum and then decrease, should become predominantly buoyancy-driven if transition occurs before the effusion rate begins to decline too rapidly.

$t^* \sim (\eta/\rho g' q^{\frac{1}{3}})^{2/(2+\alpha)}$. For the special case of fixed volume flows ($\alpha = 0$) buoyancy is the dominant driving force in their initial stages (neglecting any earlier inertial regime before the crust has developed), and it can be shown that it will remain so through time.

Similar transition from overpressure to buoyancy dominated flow can occur when the dominant stresses opposing motion arise from a uniform interior yield stress or from the crust. The time dependence of the ratio of pressure to buoyancy forces and the transition times for various cases are listed in table 2. In all cases it is assumed that $\alpha > 0$. If the strength of the crust provides the dominant resistance to motion, buoyancy can become the dominant driving force for $\alpha > \frac{3}{4}$ (for a point source) or $\alpha > \frac{1}{2}$ (for a line source). For smaller values of α the effusion rate decreases rapidly, the crust thickness increases faster than the radius of the extrusion, and the overpressure increases faster than the buoyancy component of the hydrostatic pressure, with the result that no transition occurs.

At the time of transition to the buoyancy-driven regime the depth $H^* = H(t^*)$ of the flow takes simple forms related to the controlling rheology. For example, for uniform viscous flow from a point source (see Huppert 1982)

$$H^* \sim Q^{\frac{1}{3}}(\eta/\rho g' Q^{\frac{1}{3}})^{\alpha/(\alpha+3)}, \tag{14a}$$

for uniform plastic flow (see Blake 1990)

$$H^* \sim \sigma/\rho g', \tag{14b}$$

for flow controlled by a viscous crust

$$H^* \sim Q^{\frac{1}{3}}(\eta_c \kappa^{\frac{1}{2}}/\rho g' Q^{\frac{2}{3}})^{2\alpha/(4\alpha+3)}, \tag{14c}$$

and for control by a plastic crust

$$H^* \sim Q^{\frac{1}{3}}(\sigma_c \kappa^{\frac{1}{2}}/\rho g' Q^{\frac{2}{3}})^{2\alpha/(4\alpha-3)}. \tag{14d}$$

For control by a brittle crust (14d) applies, but with the shear strength σ_c replaced by a tensile strength. If $\alpha = 1$, these transition depths reduce, in the above order, to

$$H^* \sim (Q\eta/\rho g')^{\frac{1}{4}}, \quad H^* \sim \sigma/\rho g', \quad H^* \sim (\kappa Q)^{\frac{1}{7}}(\eta_c/\rho g')^{\frac{2}{7}}, \quad H^* \sim (\kappa Q)(\sigma_c/\rho g')^2. \tag{15}$$

Reverse transitions, from buoyancy to overpressure dominated flow, are not possible for extrusions having fixed α. However, the buoyancy–crust strength regime (BCS) is not accessible if $\alpha < \frac{1}{4}$, since this static balance would require the radius to decrease with time in order that the height increase at a rate sufficient to balance the strength of the growing crust. Instead, the thickening of the crust ensures that the crust continues to support stresses greater than those due to buoyancy, and the overpressure required to force continuing effusion remains dominant.

4. Laboratory models

It is not possible to unambiguously test in laboratory analog experiments the validity of the above theoretical scaling for all of the flow regimes of interest. This is because laboratory analog flows remain complicated despite simplification of basal topography and the possibility of choosing fluids having rheologies and solidification behaviour simpler than those of lava. In particular, we have no means of predicting the effective rheology of a partly solidified or fractured crust on either wax or lava. Hence, we cannot predict the dynamical regime. On the other hand, laboratory modelling of flows involving surface cooling enables the behaviour to be measured for a range of values of many of the variables. Comparison of experimental results with the above scalings can then be used to draw conclusions about the role of the crust. Isothermal viscous and plastic extrusions (Huppert 1982; Blake 1990) provide standards with which to compare the present more complicated flows.

Measurements of the evolution of flow length and depth were taken from the same experiments previously reported in studies of flow morphology (I, II). Briefly, polyethylene glycol wax (PEG 600) was injected at a constant flow rate (hence $\alpha = 1$) onto the floor of a tank of cold water. Sugar was dissolved in the water in order to reduce the density contrast between the water and the wax. The point source was at the centre of a square tank 30 cm wide. The slit source extended across the full width of a rectangular tank 20 cm wide, 25 cm from each end wall. The tank floors were smooth plastic but, when desired, a coarse brass mesh was laid on the base to act as a rough, non-slip surface. Wax was injected at a selected temperature 1–5 °C above the wax freezing point of 18.2 ± 0.2 °C. The sugar solution was at a temperature $0 < T_a < 15$ °C. The wax viscosity at the temperature of injection varied between 1.62×10^{-4} and 1.0×10^{-4} m^2 s^{-1}, and its density was 1.126×10^3 kg m^{-3}.

Once a run began, orthogonal top and side view photographs were taken at regular intervals to record the shape of the wax extrusion and the rate of advance of the flow

front. The position of the flow front and the depth of the wax above the source were later digitized from the photographs. Since the flow front produced by radial spreading from the point source was generally not axisymmetric (a result of the development of surface crust which connected with the base at the flow front) the azimuthal average of the radius was estimated from measurements at eight equally-spaced points. Similarly, the fronts produced by two-directional spreading from the line source were not straight when crust was visible and the length of the flow (the distance from source to flow front) was determined by averaging sixteen measurements, eight equally spaced along each side of the source.

As well as carrying out runs with both point and line sources, and smooth and rough bases, a range of flow conditions were used, giving a variety of surface features (described in I and II). Because the polyethylene glycol wax is a Newtonian viscous liquid at temperatures above its freezing point and the strain rates relevant to the experiments, whereas the stresses are likely to be dominated by a yield strength at temperatures below the freezing point, we expect that the flow regimes encountered will be dominated by either a basal shear stress acting on an homogeneous viscosity in the bulk of the flow (case BNI in table 1) or a yield stress in a solidified crust (BCS or PCS). It is also possible that flow, under conditions where surface cooling takes place but solidification is slow to occur, might be controlled by a thin viscous surface layer (BNC). The experiments do not include cases in which the bulk of the extruded liquid has a finite yield strength.

5. Experimental parameters and flow morphology

Fink & Griffiths (1990, 1992) showed that a dimensional analysis of solidifying flows of a given material with constant effusion rate provides two independent dimensionless parameters. These parameters together determine the rate of surface solidification. They are the normalized temperature drop required for solidification of the surface,

$$\Theta_s = (T_\ell - T_s)/\Delta T, \tag{16}$$

(where $\Delta T = T_\ell - T_a$, and T_ℓ, T_a, and T_s are the eruption, ambient, and solidification temperatures, respectively), and the rate of cooling of the surface compared with the rate of lateral spreading of the flow (a modified Péclet number, Π). The modified Péclet number is a function of the effusion rate, the temperature difference, and the many physical properties of both the extruded fluid and its environment. It incorporates both the rate of conduction of heat within the flow and the magnitude of the heat flux from the surface owing to turbulent convection, and can readily be adjusted for the case of radiative heat transfer from the surface (Griffiths & Fink 1992*a*). It was also argued that Θ_s and the Péclet number can be combined into a single, more useful parameter Ψ, which is the ratio of the time t_s for onset of solidification of an element of lava after it is brought into contact with the environment to the timescale t_a for lateral advection of viscous fluid in the absence of cooling:

$$\Psi = t_s/t_a. \tag{17}$$

The advection timescale for constant effusion rates is given by

$$t_a = (\nu/g')^{\frac{3}{4}} Q^{-\frac{1}{4}} \quad \text{(point source)}, \tag{18a}$$

$$t_a = (\nu/g')^{\frac{2}{3}} q^{-\frac{1}{3}} \quad \text{(line source)}. \tag{18b}$$

It is useful for our present purpose to summarize the observations (discussed in I and

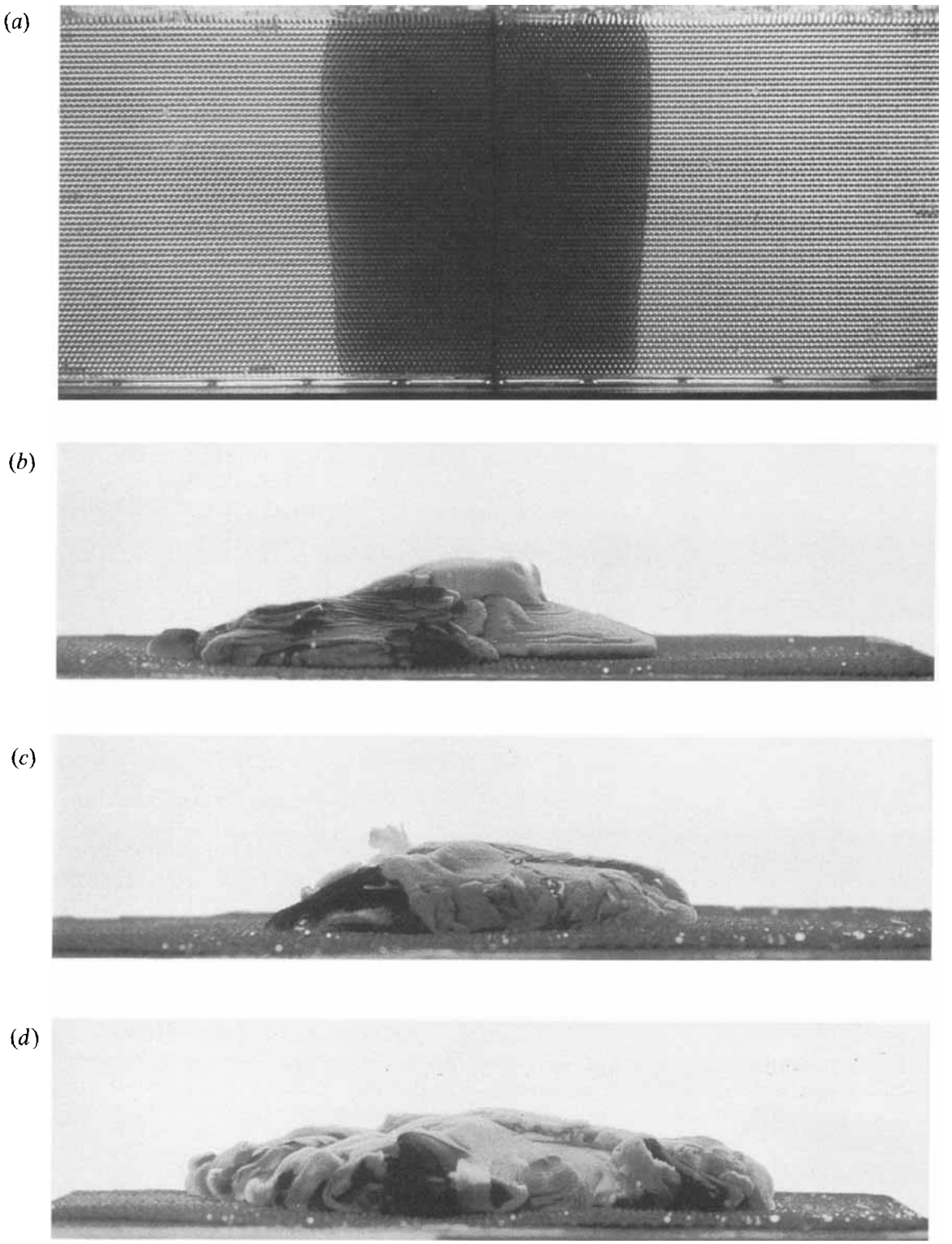

FIGURE 2(*a–d*). For caption see facing page.

(*e*)

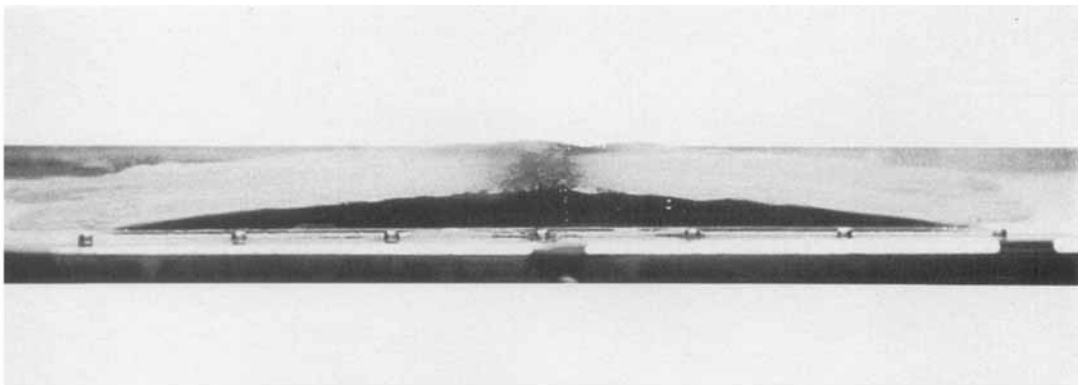

(*f*)

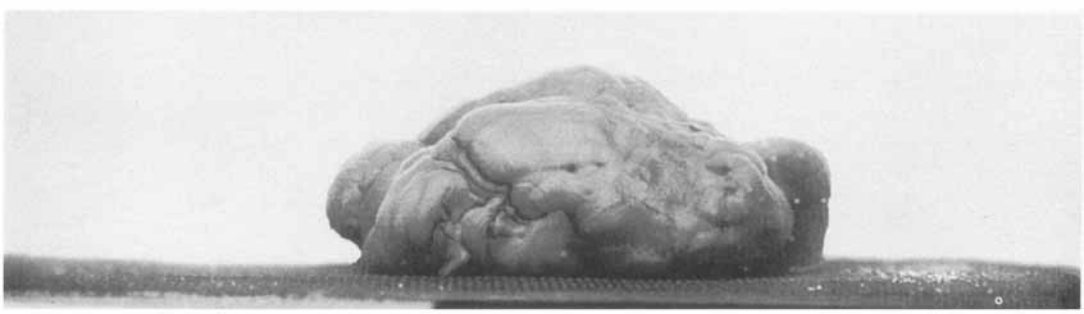

(*g*)

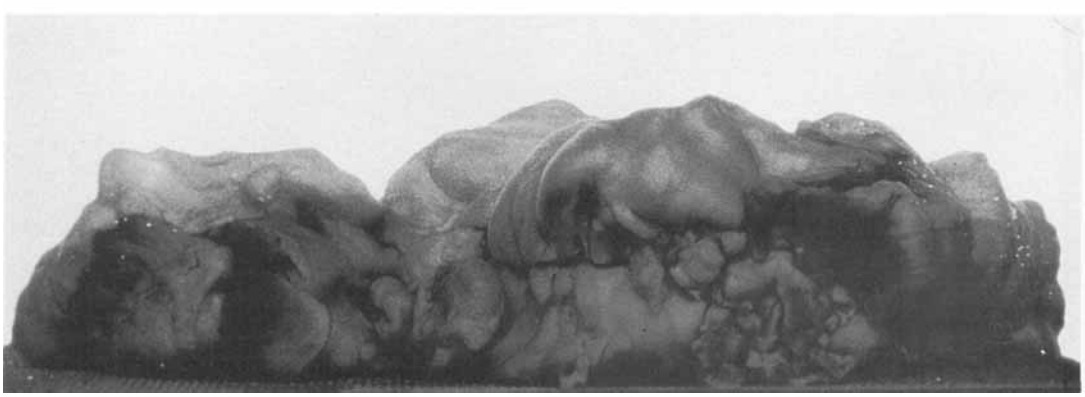

FIGURE 2. Photographs of extrusions of molten polyethylene glycol wax (grade 600) beneath cold aqueous sugar solution for different rates of surface solidification relative to effusion rate, showing different extrusion shapes and surface structure. (*a*) A plan view of flow from a line source on the rough base with $\Psi = 30$ and no solid crust; (*b*) a side view of an extrusion from a point source on a rough base with $\Psi = 16.8$ and extensive folding of the crust; (*c*), (*d*) side views of two stages of a point source extrusion on a rough base, having $\Psi = 9.0$ and spreading by 'rifting'; (*e*) a slightly oblique side view of an extrusion from a line source onto a smooth base with $\Psi = 11.3$, showing two solid crustal plates separated by a single linear 'rift' above the source; (*f*), (*g*) two stages of a point source extrusion onto a rough base, having $\Psi = 4.4$ and classified as dominantly 'pillow' with some minor 'rifting' visible at left in (*g*). The conditions in these experiments are: (*a*) experiment 114: $T_a = 14.5$ °C, $T_\ell = 19.5$ °C, $\Theta_s = 0.700$, $q = 1.7 \times 10^{-5}$ m^3 s^{-1} m^{-1}, $g' = 0.115$ m s^{-2}, photographed at $t = 227$ s after extrusion began; (*b*) experiment 133: $T_a = 11.6$ °C, $T_\ell = 19.5$ °C, $\Theta_s = 0.810$, $Q = 1.9 \times 10^{-6}$ m^3 s^{-1}, $g' = 0.110$ m s^{-2}, $t = 220$ *s*; (*c*) and (*d*) experiment 124: $T_a = 8.6$ °C, $T_\ell = 19.6$ °C, $\Theta_s = 0.855$, $Q = 4.4 \times 10^{-6}$ m^3 s^{-1}, $g' = 0.104$ m s^{-2}, $t = 117$ and 168 s; (*e*) experiment 117: $T_a = 11.5$ °C, $T_\ell = 20.0$ °C, $\Theta_s = 0.765$, $q = 1.7 \times 10^{-5}$ m^3 s^{-1}, m^{-1} $g' = 0.106$ m s^{-2}; (*f*) and (*g*) experiment 137; $T_a = 1$ °C, $T_\ell = 20$ °C, $\Theta_s = 0.895$, $Q = 9.2 \times 10^{-6}$ m^3 s^{-1}, $g' = 0.088$ m s^{-2}, $t = 102$ and 317 s.

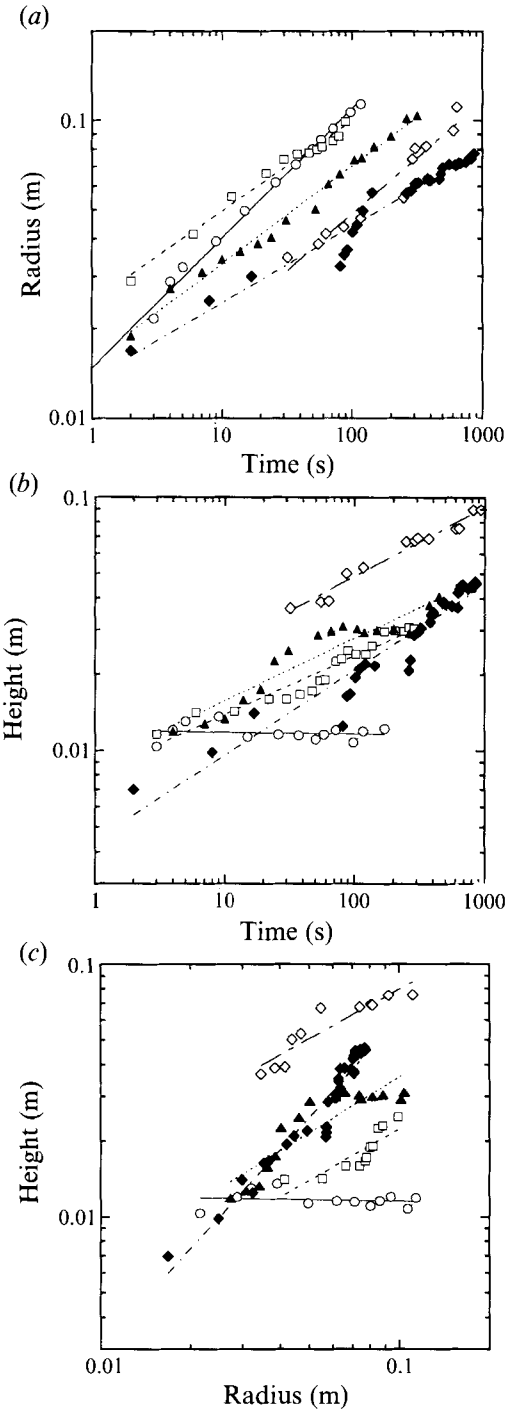

FIGURE 3. The evolution of five wax extrusions formed by a constant flux from a point source on a rough base: (*a*) the mean radius R as a function of time since the effusion began; (*b*) the maximum height H as a function of time; (*c*) the height H as a function of the mean radius. ○, $\Psi = 85$ ('no crust' regime); □, $\Psi = 23$ ('folding' regime); ▲, $\Psi = 8.1$ ('rifting' regime); ◇, $\Psi = 1.6$ ('pillows'); ◆, $\Psi = 0.40$ ('pillows'). Slopes of the lines of best fit show a progression with Ψ, excepting the run at $\Psi = 1.6$. The intercept for the lines is a function of the effusion rate.

II) of structural features. The flow morphology varied with both Θ_s and Péclet number, but over the range of variables accessible in the experiments there was a unique correspondence with the value of Ψ. For flows extruded on rough bases five morphologic types were identified. At $\Psi < 3$ (most rapid cooling) the extrusion enlarged by forming bulbous 'pillows' similar to submarine pillow basalts, and no other clearly defined structures could be seen. At $3 < \Psi < 10$ multi-armed 'rifting' of rigid crustal plates dominated, with some pillows forming at later stages of runs with a point source when the flow front had advanced far from the vent and greatly increased its perimeter length. Rifts tended to be radial at small times, but became more randomly oriented after the extrusion became large. At $10 < \Psi < 30$ the crust was relatively thin and could be buckled by compressive stresses in the flow direction. Folding gave rise to 'ropy' structure which appeared first at the flow front and later covered much of the surface (although some signs of radial rifts persisted under these conditions as well). At $30 < \Psi < 55$ crust was confined to marginal levees of solid which tended to impound the flow until they were overrun. At $\Psi > 55$ (slowest cooling or most rapid extrusion) no crust at all developed before the flow front reached the walls of the tank. Other important observations are that, when the source flux was turned off, extrusions with no solid crust continued to spread, whereas all motion stopped almost immediately for runs having $\Psi < 30$. This suggests control by a yield strength. At $\Psi < 3$ existing small outbreaks sometimes continued flowing for a few seconds after the source flux stopped, apparently relieving pressure within the extrusion. This suggests that overpressure was significant.

It is not clear whether the same sequence of morphologies or the same transition criteria as observed in the wax experiments will apply to lava flows. Effusion rates and magma viscosities are poorly known. However, first attempts to test this correspondence show that a range of lavas, from large basalt flows to small lava domes and individual underwater 'pillows', are all consistent with the laboratory results (Griffiths & Fink 1992*a*, *b*). In the following sections we again present results in terms of the value of Ψ. Their dependence on Θ_s and Π have also been considered. Much of the variation of Ψ between runs is due to differing values of Θ_s and the graphs appear much the same when data are plotted against Θ_s instead of Ψ. However, runs with the largest differences in effusion rate indicate also a dependence on the Péclet number: smaller effusion rates lead to flows which have more time to develop thicker crust, tend to have larger aspect ratios H/R and experience greater disruptions to continuous advance of the flow front. Within the experimental uncertainties the single parameter Ψ gives a satisfactory, unique identification of the flow conditions and behaviour.

6. Experimental results

The photographs in figure 2 illustrate the considerable variations in shape of extrusions and the appearance of their surfaces over the range of Ψ achieved. (Plan-view photographs of similar runs can be found in I and II.) These qualitative differences are reflected in the spreading relationships, examples of which are given in figure 3 (point source) and figure 4 (line source). For the point source, measurements were taken only from runs with a rough base, none of which lay in the range $30 < \Psi < 80$, where solid is confined to levees at the flow front.

6.1. *Trends with time*

For large values of Ψ ($80 < \Psi < 500$) no visible solid developed on the surface before the flow front reached the endwalls of the tanks, and the front was close to

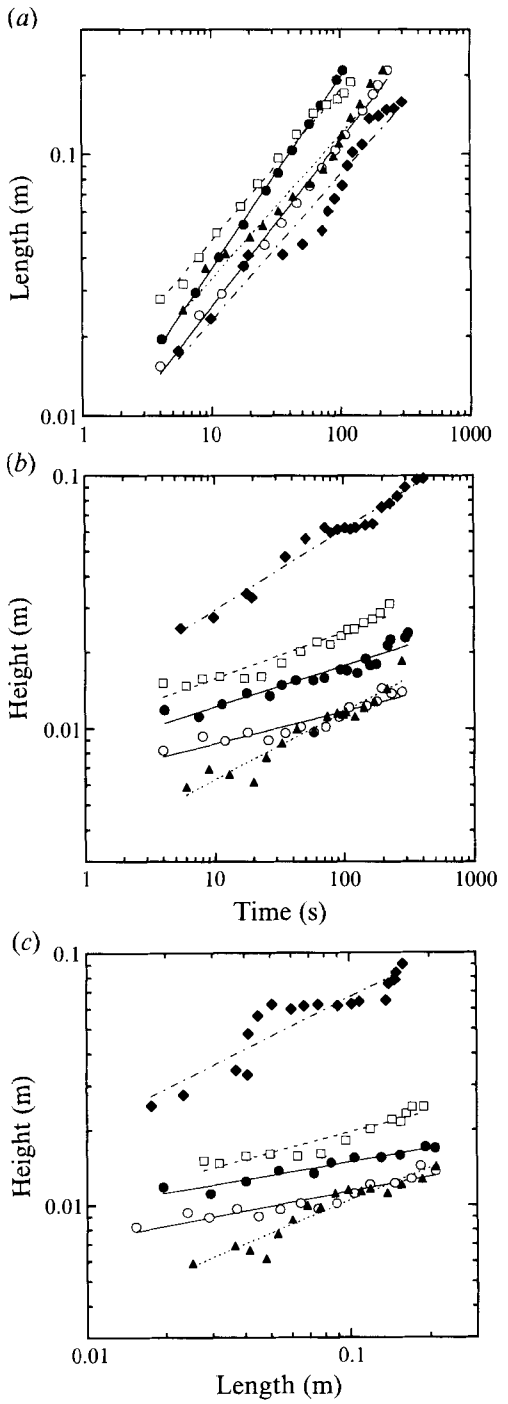

FIGURE 4. The evolution of five wax extrusions formed by constant effusion rates from a line source: (*a*) the mean length L as a function of time since extrusion began; (*b*) the maximum height H as a function of time; (*c*) the height H as a function of the length L. ●, $\Psi = 524$ ('no crust' regime); ○, $\Psi = 30.0$ ('no crust'), □, $\Psi = 8.2$ ('folding'); ▲, $\Psi = 4.0$ ('rifting'); ◆, $\Psi = 1.8$ ('pillows'). Note the progression with Ψ of slopes of the lines of best fit. Intercepts depend on effusion rate.

axisymmetric in the case of a point source, or straight and parallel to the line source (as shown in figure 2*a*). The extrusion radius or length increased in a smooth, monotonic fashion (see figures 3*a* and 4*a*) according to the simple power laws $R \sim t^{0.50 \pm 0.09}$ (four runs on a rough base) and $L \sim t^{0.74 \pm 0.04}$ (three runs on smooth and rough bases), where the exponents are averages and mean deviations. For the same runs the depth of the flow from the point source (figure 3*b*) tended to remain very nearly constant ($H \sim t^{0.03 \pm 0.03}$) after a 2–3 s start-up phase, while the depth of flows from the line source (figure 4*b*) increased with time as $H \sim t^{0.14 \pm 0.03}$.

Although the exponents for both L and H in the line source cases at large Ψ are slightly less than those predicted for regime BNI (table 1), the results for both sources are consistent with those predicted for isothermal viscous spreading. The small discrepancy for line sources may be due to cooling because the wax was intruding beneath water which was at a temperature below the wax solidus and a more viscous (but not solid) surface layer may have formed. The powers are slightly larger for the smooth base than for the rough base, suggesting that the effective loss of some of the spreading fluid into the roughness elements in the rough base may have contributed to slower spreading and deepening. We conclude that the wax flows having $\Psi > 80$, at least over the times taken by the flow front to reach the tank walls, were buoyancy-driven and controlled by basal shear stress acting on a uniform Newtonian viscosity.

At intermediate values of $\Psi (3 < \Psi < 30)$, where solid crust formed into transverse folds (shown in figure 2*b*) or mobile rafts of rigid crust separated by rift-like features (figure 2*c*, *d*) spreading was not axisymmetric nor uniform along the line source, because the crust joined onto the rough base at the flow front and temporarily impeded, or even halted, the flow at some places. At other times and other positions along the front the flow advanced by deforming the crust, pushing it away or, at Ψ near 30, by building up behind and flowing over it (see the outflow to the left in figure 2(*b*), and the fresh break-out taking place to the left in figure 2(*c*)). Taking the average radius or length removes most of the resulting irregularity. The average radius increases in a manner that is in some cases smooth and of constant slope against logarithmic axis scales. However, in other cases it shows up to six changes in slope (figures 3*a* and 4*a*). These changes are correlated with even more noticeable variations on the plots of maximum depth versus time (figures 3*b* and 4*b*) and depth versus length (figures 3*c* and 4*c*): within a run the depth tends to increase more rapidly at times when the radius is increasing more slowly. On the other hand, over the duration of a run these data too are reasonably described by simple power laws. There are also clear trends between runs: at the smaller values of Ψ the radius or length increases less rapidly with time, the depth increases more rapidly with time, and the aspect ratio H/R is larger. The larger aspect ratio is associated with a deeper flow front at smaller Ψ, as is clearly seen in the sequence in figure 2.

The presence of a rough base (in either source geometry) forces the crust to fracture or deform in order for the flow front to advance. In addition, azimuthal divergence in flow from a point source leads to divergence of fragments of crust and exposure of more melt. These effects are considerably reduced when flow emerges from a line source onto a smooth base. In that case the solid crust tends to form a relatively smooth plate on each side of the source, with a single rift above the source (figure 2*e*). The solid at the flow front slips over the smooth base and exerts less resistance to motion.

At very small values of $\Psi (\Psi < 3)$ solid crust developed immediately over the vent and formed a thick shell over the flow (figure 2*f*, *g*). At small times (figure 2*f*) these flows were balloon-like, being roughly equi-dimensional and not far from circular in

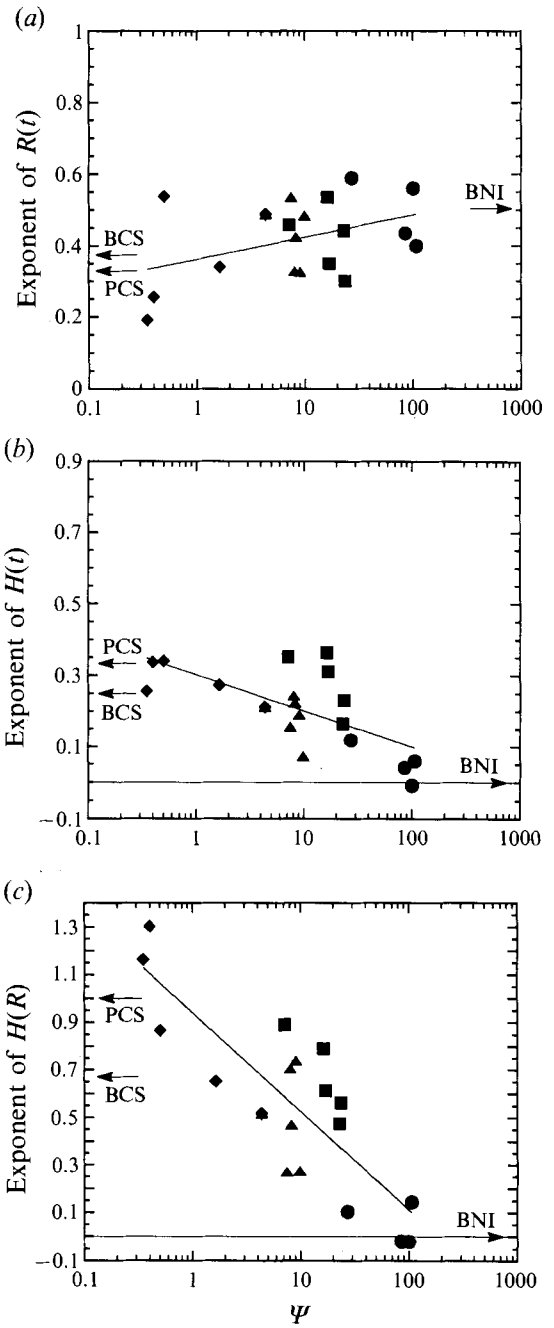

FIGURE 5. Exponents of simple power-law fits to the radius and height of extrusions for each run with the point source, on a rough base, as a function of the solidification parameter Ψ. Power laws are fits to (*a*) $R(t)$, (*b*) $H(t)$, and (*c*) $H(R)$. Symbols indicate independent morphologic classifications: ●, 'no crust' regime; ■, 'folding'; ▲, 'rifting'; ◆, 'pillows'. The straight line (a logarithmic fit) is intended only to indicate the trend, and does not imply that a variation of this simple form is expected. Arrows indicate the exponent predicted for isothermal buoyancy–viscous gravity currents (BNI in table 1), the buoyancy–crust yield strength balance (BCS) and the overpressure–crust strength balance (PCS) for constant effusion rate.

vertical section. At this stage the extrusion was one 'pillow' that enlarged until the crust broke and a second pillow developed. Melt subsequently flowed out from further fractures or weak spots in the crust to form many bulbous lobes reminiscent of pillow basalts. A large dome was eventually built up of the bulbs (figure 2*g*). Dissection of such a dome showed that the solid formed many interconnected cavities through which melt could flow. Under these conditions the spreading was far from smooth and variation of the depth was not monotonic in time, sometimes decreasing during periods when the radius increased fastest (figures 3 and 4). Such intermittent and non-uniform growth leads to many kinks in plots such as those in figures 3 and 4. It is not entirely satisfactory to simplify this behaviour as a power law in runs where there are only two or three kinks. However, we proceed to do so in order to obtain an estimate of the overall behaviour. The power laws found by regression for each experiment continue the trend noted above: the radius tends to increase less rapidly and the depth more rapidly than they do at larger values of Ψ.

6.2. *Trends with Ψ: point source*

The power law exponents for $R(t)$, $H(t)$ and $H(R)$ from the point source experiments are summarized in figure 5, where the data are also coded according to our previous classification of flow morphology (I). The scatter is a natural consequence of the complexity of the spreading and our ability to find the gross behaviour from a record of limited duration. However, the trends are clear in figure 5 and we represent them using straight lines because no more complicated form is justified by the data. The variations of greatest experimental significance are those in $H(t)$. The powers range from the values predicted for buoyancy–viscous flow (these are found at $\Psi > 80$) to those predicted for flow dominated by overpressure and crust strength (found at $\Psi < 3$). Note that these powers alone cannot distinguish between homogeneous viscous flow at large Ψ and one controlled by the viscosity of a thin crust (see table 1, with $\alpha = 1$). For small Ψ, observation revealed that the crust did indeed act as a brittle solid, appearing to control the advance of the front. At intermediate values of Ψ the data are consistent with the predictions for the 'intermediate' regime in which buoyancy is balanced by crust strength, and this too is consistent with qualitative observations of the crust, along with the immediate cessation of motion after the source flux was turned off.

The dynamical models of table 1 also predict the dependence of radius and depth on the effusion rate, denoted Q when $\alpha = 1$. In order to compare with the data we plot the coefficient β in (9) found for a number of the runs using a point source. Since β may be a function of both the effusion rate and thermal conditions (the latter affecting material properties) it is necessary to compare runs having similar values of Θ_s. From figure 6 we see that four runs having $\Psi > 80$ (three at $\Theta_s = 0.69$ and one at $\Theta_s = 0.80$) give intercepts which increase with Q in a manner consistent with $\beta \sim Q^{\frac{1}{4}}$ (although we cannot discount the relation $Q^{\frac{1}{7}}$ predicted for viscous crust). The fourth point having different Θ_s can be included here because these runs all showed no signs of solid crust. In contrast, four runs having $\Theta_s = 0.80$–0.824 and four having $\Theta_s = 0.853$–0.863, and all clearly in the intermediate 'folding' or 'rifting' morphologic regimes, respectively, all show intercepts which decrease with increasing Q consistent with $\beta \sim Q^{-\frac{1}{3}}$. These opposite trends are as predicted in table 1 (with $\alpha = 1$) for homogeneous buoyancy–viscous flows on the one hand and a buoyancy–crust strength balance on the other. The result that larger effusion rates or slower cooling give smaller flow depths for the intermediate Ψ values is also evidence that the effective thickness of strong crust increases with time.

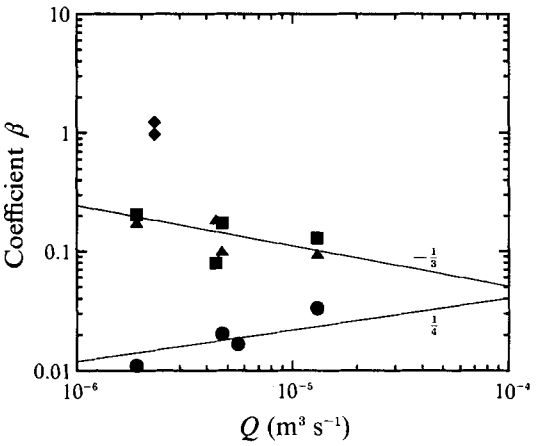

FIGURE 6. The coefficients β (in SI units $m^{1-\lambda}$, where λ is the exponent of the power law) found by fitting the simple power law (9) to runs from a point source on a rough base: ●, runs with large values of Θ_s (0.686 to 0.797), a range of effusion rates Q, and morphology in the 'no crust' regime; ■, runs with $\Theta_s = 0.81$ to 0.82 and 'folding' crust; ▲, runs with $\Theta_s = 0.85$–0.86 and 'rifting' morphology; ◆, runs with $\Theta_s = 0.971$ and 0.974, and 'pillow' morphology. Lines shown have slopes $\frac{1}{4}$ and $-\frac{1}{3}$ predicted for dynamical regimes BNI and BCS in table 1.

Intercepts from two runs having the largest Θ_s and smallest Ψ are also shown in figure 6. They plot close to one, as is predicted for the overpressure dominated regime. The source of the dominant retarding stress in this pressurized regime cannot be deduced from the data, it can only be hypothesized: if the crust thickness increases as the square root of time, viscous stresses will give way to crust strength after a time given by (11); also, if the crust strength is dominant at intermediate Ψ, then it is likely to be dominant at these smaller values of Ψ.

An estimate of the magnitude of the effective yield strength of the wax crust can be obtained from the measurements of extrusion height. We select runs having $3 < \Psi < 10$, assume these are dominated by a balance between buoyancy and crust strength, and fit the power law $H \sim \phi t^{\frac{1}{4}}$ to the data (see table 1, regime BCS). From the form of the coefficient ϕ we find $\sigma_c \approx \rho g' \phi^2 \kappa^{-\frac{1}{2}}$ (up to a constant of order one). The fit gives $\sigma_c \sim 40$ (± 20) Pa.

6.3. *Trends with Ψ: line source*

The power law indices for length and height in line source experiments are collated in figure 7, and are again coded by the previous morphologic classification (II). Powers for $L(t)$ again tend to decrease slightly with decreasing Ψ (from 0.74 to 0.58). Given the predicted powers of 0.8, 0.75 and 0.5 for line source regimes BNI, BCS and PCS, respectively (table 1), these results are broadly consistent with the dynamical regimes suggested by the point source experiments. However, the variations with Ψ are less obvious than they were in the point source runs, and their interpretation is inconclusive. One complication is that a majority of the line source experiments at $\Psi < 100$ exhibit a change of slope during the run, generally at times of order 20–30 s. These changes are most clearly identified in the data for flow depth. Therefore we plot in figures 7(*b*) and 7(*c*) the slope of power laws fitted to data at times after the apparent transition, along with an arrow showing the slope at small times and the direction of the change. For runs with a rough base and small values of Ψ (where spreading is through 'pillow' formation) slopes tend to change from a large to a smaller value. At larger Ψ, on the other hand, the change is smaller and in the opposite direction: a nearly constant depth

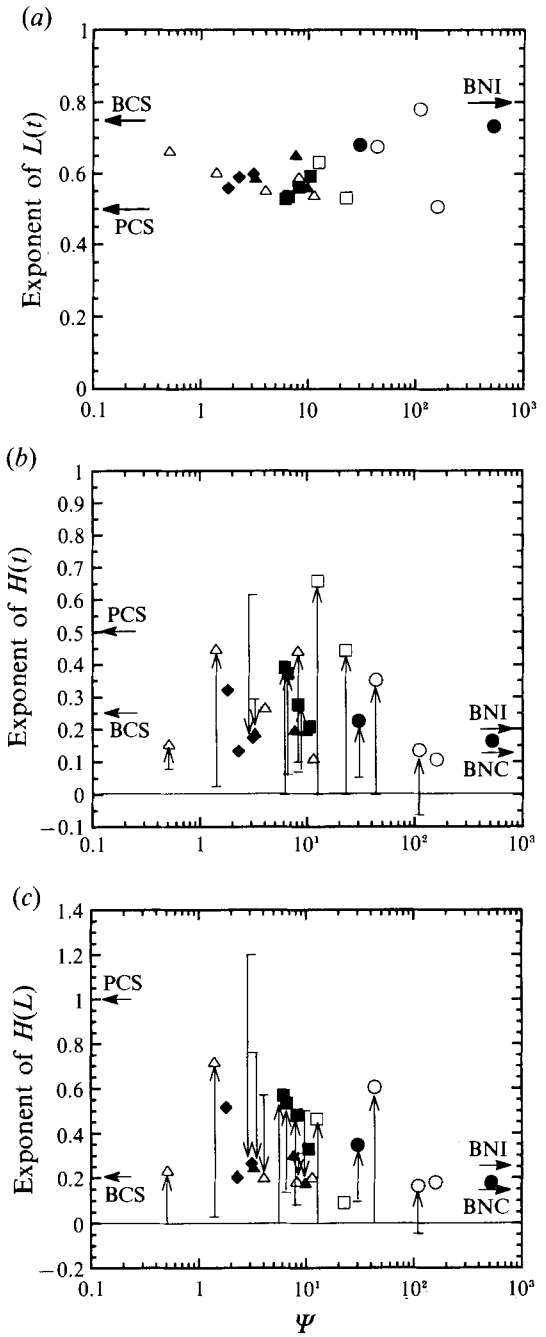

FIGURE 7. Exponents of power laws fitted to length and height measurements for each run from a line source. Filled symbols are for runs on a rough base, open symbols for a smooth base; ●, ○, 'no crust'; ■, □, 'folding'; ▲, △, 'rifting'; ◆, ◇, 'pillows'. Where the early and late stages of a run appear to show a distinct difference in power law the exponent for small times is plotted as a dash, the exponent for large times as a symbol, and the two are connected with an arrow indicating the direction of change. Power law curves are fits to (*a*) $L(t)$, (*b*) $H(t)$, (*c*) $H(L)$. Horizontal arrows indicate the exponents predicted for regimes BNI, BNC, BCS and PCS (table 1) with constant effusion rate ($\alpha = 1$).

at small times gives way to a more rapid increase in depth and a slower decrease of the aspect ratio H/L at large times. In the narrow band $5 < \Psi < 10$ both slope changes occur, as do both the 'folding' and 'rifting' morphologies. Indeed, the direction of change of the slope correlates perfectly with the morphologic classifications: only those runs in which the dominant surface feature was 'folding' or 'no crust' show a transition to larger slope, whereas only runs classed as 'rifting' or 'pillows' show a decrease in slope. The behaviour is the same for runs on a smooth base, apart from two runs at very small Ψ. In these two runs the crust did not attach itself to the base, tended to slide forward, and the 'pillow' regime was not seen (II).

Despite the above complications the data from the line source are consistent with the scaling solutions for the following dynamical regimes. At $\Psi > 100$ extrusions are homogeneous buoyancy–viscous gravity currents (regime BNI) and are not affected by surface cooling during the time taken for the front to reach the sidewalls of the tank (a distance of order 25 flow depths). At $10 < \Psi < 100$ (or at $\Psi > 5$ if transverse folding is the dominant form of crust deformation) the wax extrusions again appear to be controlled at small times by buoyancy forcing and viscous shear stresses. However, powers for $H(t)$ and $H(L)$ are consistently smaller than those found at larger Ψ and for the isothermal viscous flows of Huppert (1982). This implies a higher viscosity of a cooled surface layer near the flow front. When crust viscosity is dominant over the interior viscosity, the predicted powers are $\frac{1}{8}$ for $H(t)$ and $\frac{1}{7}$ for $H(L)$ in place of $\frac{1}{5}$ and $\frac{1}{4}$ for isothermal flows. In these runs the onset of solidification occurs a significant distance from the vent and extrusions do not have solid crust during their early stages. Later development of solid crust on these flows leads to a transition into a regime in which the powers are relatively large (mean of 0.3 ± 0.1 for $H(t)$ and 0.4 ± 0.06 for $H(L)$). These are greater than any predicted for a purely buoyancy-driven flow and indicate that flow in the new regime is probably driven by both buoyancy and overpressure, and resisted by a crustal strength. At $\Psi < 5$ and small times $H(t)$ has a power close to $\frac{1}{2}$ and $H(L)$ a power close to one, as expected if overpressure provides a dominant contribution to the driving forces at small times. At large times the runs with small Ψ give much smaller powers (0.17 ± 0.06 for $H(t)$ and 0.21 ± 0.03 for $H(L)$) which support the buoyancy–crust strength model.

6.4. *Regime transitions*

Regime transitions could be identified for line sources but not for point sources. There are several possible reasons for this. First, transitions may have been masked by the many irregularities in spreading with solidifying crust. Note that if overpressure is replaced by buoyancy as the dominant driving force while opposed by the strength of a thin crust, the predicted power laws for $H(R)$ in the point source case change from $H \sim R$ to $H \sim R^{\frac{2}{3}}$, whereas for a line source $H(L)$ undergoes the much greater change from $H \sim L$ to $H \sim L^{\frac{1}{5}}$. For the same reason transitions would not be obvious in plots of radius against time. Similarly, a change from a homogeneous viscosity to a more viscous crust (BNC) leads to no change in the power laws predicted for radial spreading from point sources but to a significant change for line sources.

Secondly, the predicted time elapsed before overpressure gives way to buoyancy is much more sensitive to parameter values in the case of a point source than it is for a line source (table 2). This difference is particularly acute if crust strength provides the dominant retarding force: for $\alpha = 1$ the transition times are $t^* \sim (\sigma_c \kappa^{\frac{1}{2}}/\rho g' Q^{\frac{2}{3}})^6$ and $t^* \sim (\sigma_c \kappa^{\frac{1}{2}}/\rho g' q)^2$, respectively. Substituting typical values (for wax $\kappa = 10^{-7}$ m^2 s^{-1}, $\rho = 1.12 \times 10^3$ kg m^{-3}, $g' = 0.1$ m s^{-2}, $q \sim (2\text{–}5) \times 10^{-5}$ m^2 s^{-1} and $Q \sim (2\text{–}5) \times 10^{-6}$ m^3 s^{-1}) for the known variables in runs with a line source and small Ψ, and a transition time

of 30 s, gives an estimate of the yield stress: σ_c (or γ_c) $\approx$ 40–100 Pa. (Note that the lower value is identical to that found earlier from the evolution of the extrusion height for intermediate Ψ.) Employing this estimate of σ_c in the expression for the transition time in point source experiments gives $t^* \sim 10^{-2}-30$ s. Hence this transition would occur too early to be detected in most of our point source experiments, and the overpressure regime should be seen for only larger values of σ_c, which are most likely at small Ψ.

A third reason for the absence of regime transitions in point source experiments concerns a finite time elapsed before onset of solidification at the surface, a factor not included in the scaling analyses. At intermediate to large values of Ψ the onset of solidification in radial flow occurs when the flow front is closer to the vent (at a radius $\sim \Psi^{\frac{1}{2}}$) than is the case for a line source (where solid forms at a distance $\sim \Psi$(II)). It is probable that the transition between viscous and plastic crust detected in the line source experiments for intermediate-to-large Ψ occurs at a time determined by the onset of solidification, rather than at the time (12) for transition to crust control predicted on the basis of a constant effective yield stress for a surface layer. In fact, if the transition time is mistakenly taken to be given by (12) (using $q \sim 5 \times 10^{-5}$ m^2 s^{-1}), we obtain $\sigma_c \sim 0.05$–0.15 Pa depending on the flow rate. A similar value was found from point source experiments under the assumption that a possible transition was that predicted for a homogeneous Bingham fluid. However, the correct value for a thin crust is likely to be close to the value 40 Pa found above. This value also gives consistency between the predicted depthscale $H^* \sim (\kappa/q)^{\frac{1}{2}}(\sigma_c/\rho g') \sim 1.5$ cm and the measured depths of approximately 1 cm at the transition time. Note that if this yield stress were uniform throughout the depth of the flow, and not confined to a thin crust, it would support an unrealistic dome height (14*b*) of 36 cm.

7. Comparison with lava flows

A test of the geologic relevance of the scaling relationships and their correspondence with flow morphology requires a comparison of the model results with measurements from actual lava flows. Very few data sets are available with enough spatial and temporal resolution to allow such evaluations. For the case of radial flow there are only two we are aware of: the lava domes that grew at Mount St Helens from 1980 to 1986 (Swanson & Holcomb 1990) and at Soufrière at St Vincent in 1979 (Huppert *et al.* 1982). These domes differed in both their compositions and eruptive styles. The dacite of Mount St Helens, pictured in figure 8, was emplaced episodically through more than 15 separate pulses over the six-year period. Its longterm effusion rate averaged over periods of activity and repose was therefore much smaller than the actual rate during the eruptive episodes themselves. In contrast the andesite of Soufrière was erupted continuously in about 200 days, with an initial phase of rapid effusion followed by a long period of steadily decreasing effusion rate.

Taking average effusion rates, and magma viscosities estimated on the basis of the composition, values of Ψ for these domes have been evaluated (Griffiths & Fink 1992*a*): for Mount St Helens $\Psi \sim 1$ and for Soufrière $\Psi \sim 2$. These values lie in the 'pillow' regime defined by the wax experiments, but close to the transition to 'rifting'.

7.1. *Mount St Helens*

Foreseeing that the Mount St Helens dome is probably controlled by a yield strength, we treat its episodic growth in terms of a small continuous effusion rate. A yield strength control implies that the dome is always in a static balance and that (as shown

FIGURE 8. The lava dome at Mount St Helens, 11 September 1981. Note crease structure (whose axis is about 30 m long) over the vent of the September 1981 lobe indicating 'rifting' behaviour. Photo courtesy of US Geological Survey Cascades Volcano Observatory.

by measurements) no significant slumping occurs between pulses. Under this assumption the dome volume is well described, over almost all of its history, by a single power law (figure 9*a*):

$$V \sim 4.66t^{0.88}, \quad 70 < t < 2200 \text{ days}, \tag{19}$$

where V is the volume in m^3 and t is the time in seconds (Swanson & Holcomb 1990; Fink, Malin & Anderson 1990). The first data point has been omitted from the regression, the effusion rate apparently being smaller during a short initial period. Thus we determine that $\alpha \approx 0.88$. The record could, arguably, be subdivided at $t \sim 1000$ days, in which case the volume grows linearly during the preceding 900 days and more slowly ($V \sim t^{0.53}$) over the succeeding 1200 days. However, we have checked that this choice makes little difference to our conclusions and we use the simpler description. Likewise, single power laws provide satisfactory descriptions of the individual quantities: dome radius (taken as half the average of the longest and shortest dimensions) as a function of time elapsed after the start of the extrusion (figure 9*b*); dome height as a function of elapsed time (figure 9*c*); and height as a function of the radius (figure 9*d*). The best fits (in SI units) are:

$$R \sim 10.4t^{0.24}, \quad H \sim 1.45t^{0.28}, \quad H \sim 0.105R^{1.14}. \tag{20}$$

We compare these descriptions of the measurements with the predictions of the scaling relations in table 1 for $\alpha = 0.88$. The exponents for the power laws are summarized in table 3. Both the isothermal viscous model and the viscous crust model (regimes BNI and BNC) predict that height decreases with time and radius, and that radius increases as $R \sim t^{0.45}$. Hence these models are not consistent with the measurements. The isothermal Bingham model, too, predicts a height increase that is

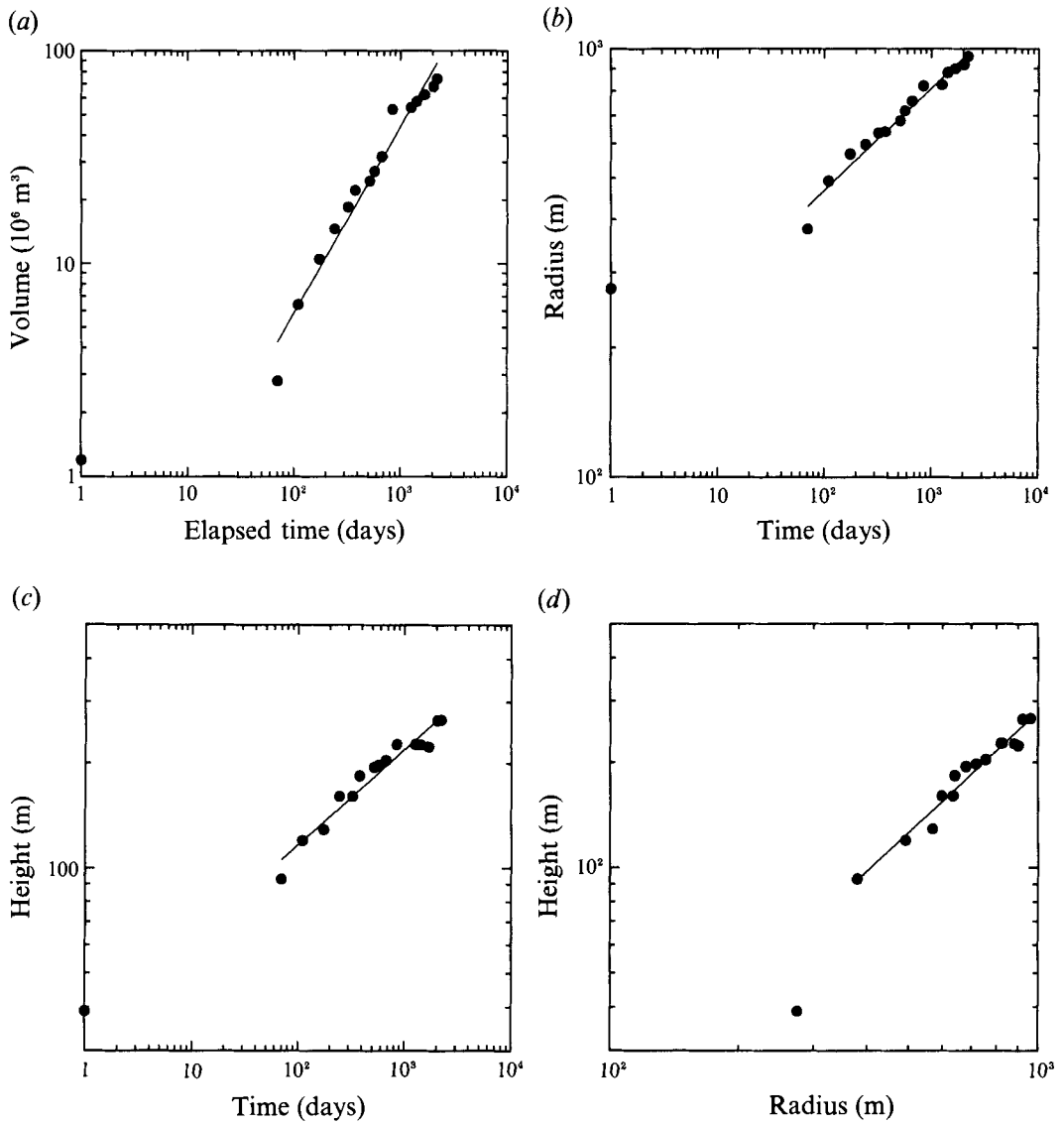

FIGURE 9. Data for the growth of the Mount St Helens lava dome from 23 October 1980 (day 1) to 12 November 1986 (day 2194). In (*a*) the accumulated volume is well described by a single power law curve (19), as shown, if the measurement on day 1 is disregarded. Thus we restrict our attention to the period $70 \leqslant t \leqslant 2194$ days. For the same period power law curves are fitted to the data for dome radius (*b*), height (*c*), and the height as a function of the radius (*d*). The best fits shown are those in (20). Data from Swanson & Holcomb (1990).

too slow ($H \sim t^{0.176}$ and $H \sim R^{0.5}$) and a radius increasing too rapidly ($t^{0.352}$). In closer agreement with the data are the model for flow driven by buoyancy and controlled by a yield strength of the crust (regime BCS: $R \sim t^{0.315}$, $H \sim t^{0.25}$, $H \sim R^{0.794}$), and the model in which overpressure balances the strength of the crust (regime PCS: $R \sim t^{0.293}$, $H \sim t^{0.293}$, $H \sim R^{1.0}$). We also find that the transition (11) from interior viscous control to crust control should occur before $t = 70$ days for $\sigma_c > 1 \times 10^3$ Pa (assuming viscosity $\eta \sim 10^8$ Pa s for the interior magma and thermal diffusivity $\kappa = 10^{-6}$ m^2 s^{-1}), a value well below the expected strength ($\sigma \sim 10^4$–10^6 Pa) for the interior magma and

	Regime	$R(t)$ exponent	$H(t)$ exponent	$H(R)$ exponent
	Mount St Helens dome ($70 < t < 2200$ days)			
BNI	Homogeneous buoyancy/viscous	0.455	−0.030	−0.066
BPI	Homogeneous buoyancy/plastic	0.352	0.176	0.5
BNC	Buoyancy/crust viscosity	0.449	−0.017	−0.038
BCS	Buoyancy/crust yield strength	0.315	0.25	0.794
PCS	Overpressure/crust tensile strength	0.293	0.293	1
Measured		0.24	0.28	1.14
	Soufrière dome ($t < 20$ days)			
BNI		0.748	0.165	0.221
BPI		0.664	0.332	0.5
BNC		0.783	0.094	0.120
BCS		0.705	0.25	0.355
PCS		0.553	0.553	1
Measured		0.76	0.35	0.47
	Soufrière dome ($40 < t < 150$ days)			
BNI		0.289	−0.141	−0.487
BPI		0.175	0.087	0.5
BNC		0.259	−0.080	−0.311
BCS		0.094	0.25	2.67
PCS		0.146	0.146	1
Measured		0.13	0.21	1.5

TABLE 3. Exponents of the power laws predicted for the various dynamical regimes of table 1 when those results are applied to the Mount St Helens and Soufrière lava domes. The predicted exponents for evolution of radius R and height H are obtained by substituting the volume exponent α (derived from data for these lava domes) into the relations in table 1. Exponents deduced from the data are given for comparison. Note that very different evolutions, but similar dynamics, are predicted from the different values of α obtained for the two stages of the Soufrière dome.

therefore much smaller than the strength of a solidified crust. Hence we predict that the dominant retarding stress throughout the period $70 < t < 2200$ days is provided by crust strength.

The presence of a static balance involving a yield strength enabled Iverson (1990) to draw conclusions about the driving forces for this dome from its shape alone, without coupling its rate of emplacement to the evolution of the thermal boundary layer. Best agreement with calculated shapes was obtained with a significant contribution from overpressure, but with buoyancy as the dominant force. We reach the same conclusion, noting that the aspect ratio $H/R \approx 0.27 \pm 0.03$ (nearly constant throughout the record), which is smaller than the aspect ratio expected for growth dominated by overpressure. It is similar to those measured in wax experiments where crust strength is thought to be balanced by buoyancy.

It is possible to estimate the effective yield strength of the crust of the Mount St Helens dome. If buoyancy is the dominant driving force (regime BCS in table 1) during most of the observation period then the coefficient of a $\frac{1}{4}$-power law fit to the data for dome height (figure 9*c*) provides the best estimate: thus $\sigma_c \sim (1.3 \pm 0.2) \times 10^8$ Pa. This result is consistent with the estimate (from table 2) that the transition from overpressure (PCS) to buoyancy-driven flow (BCS) occurs within a time of order

1000 days only if the crust strength (using $\kappa = 10^{-6}\ \mathrm{m^2\ s^{-1}}$, $\rho = 2.6 \times 10^3\ \mathrm{kg\ m^{-3}}$) $\sigma_c < 3 \times 10^8$ Pa. (A greater strength would have given overpressure dominance throughout the growth.) With the retarding stress provided by crust strength, the predicted dome height (14 *d*) at transition is $H^* < 12$ m, which is less than the height of the Mount St Helens dome at day 1 of the growth record. Keeping in mind that numerical constants of order one for each of the theoretical relations in table 1 remain unknown, the above results all imply a dominance of buoyancy and crust strength, with overpressure probably significant early in its growth. Iverson (1990) considered the tensile strength. However, we suggest that the small aspect ratio indicates a significant role for shear stress, and that the highly fractured crust is likely to undergo plastic deformation.

7.2. *La Soufrière*

Calculations of the volume of the dome in La Soufrière (Huppert *et al.* 1982) show that it increased most rapidly during the first 20 days, after which the extrusion rate steadily decreased. As shown in figure 10(*a*), the history is very closely described by two power laws:

$$V \sim 5.18 \times 10^{-4} t^{1.66} \quad (1 \leqslant t \leqslant 20 \text{ days}),$$

$$V \sim 3.75 \times 10^{4} t^{0.437} \quad (40 < t < 150 \text{ days}), \tag{21}$$

(where the coefficients are again in SI units). The break after 20 days of growth gives a better characterization of the available data than does the break at 90 days employed by Huppert *et al.* (1982). For the first stage of growth the exponent in (1) is $\alpha = 1.66$, and for the second stage $\alpha = 0.44$. The data for dome radius (figure 10*b*) and height (figure 10*c*, *d*) also reveal the same two stages, which we discuss separately.

For the first 20 days of growth of the Soufrière dome the data indicate:

$$R \sim 5.6 \times 10^{-3} t^{0.76}, \quad H \sim 0.56 t^{0.35}, \quad H \sim 6.2 R^{0.47}. \tag{22}$$

Substituting $\alpha = 1.66$ into the relations in table 1 we find the exponents listed in table 3. The predicted powers for $R(t)$ in the two viscous models (BNI and BNC) are 0.75 and 0.78, which are similar to the data. However, the same models predict powers of 0.165 and 0.094 for $H(t)$, along with 0.221 and 0.120 for $H(R)$, all much smaller than those observed. For the overpressure regime, on the other hand, a variation of radius that is too slow ($R \sim t^{0.55}$) and variation of height that is too rapid ($H \sim t^{0.55}$, $H \sim R^{1.0}$) are predicted. Only predictions of models in which buoyancy is balanced by a yield strength (BPI and BCS) satisfactorily match the observations: from the homogeneous plastic model $R \sim t^{0.66}$, $H \sim t^{0.33}$ and $H \sim R^{0.5}$, whereas the thin crust model predicts $R \sim t^{0.705}$, $H \sim t^{0.25}$ and $H \sim R^{0.355}$.

Blake (1990) showed that the homogeneous Bingham plastic model provides a better fit to the second stage of growth of this dome than does the isothermal viscous model. For the first stage, however, we cannot say from the data whether the homogeneous model or the crust model (both in balance with buoyancy) provides the better description – the measurements suggest the dome was controlled by a combination of the two strengths. We note the yield strengths indicated: from the coefficient obtained by fitting the predicted form for $H(t)$ (table 1) we find $\sigma \sim 2.8 \times 10^5$ Pa if the interior strength is dominant (cf. Blake's value $\sigma \sim (2.6 \pm 0.5) \times 10^5$ Pa obtained for the second stage) or $\sigma_c \sim 8 \times 10^6$ Pa if the crust provides the primary retarding force. Although both the homogeneous and crust models cannot be precisely valid at the same time, taking the strengths implied by these two models at face value gives $\sigma_c/\sigma \sim 30$, from which (10) implies that the crust dominance can be valid only if the crust thickness is

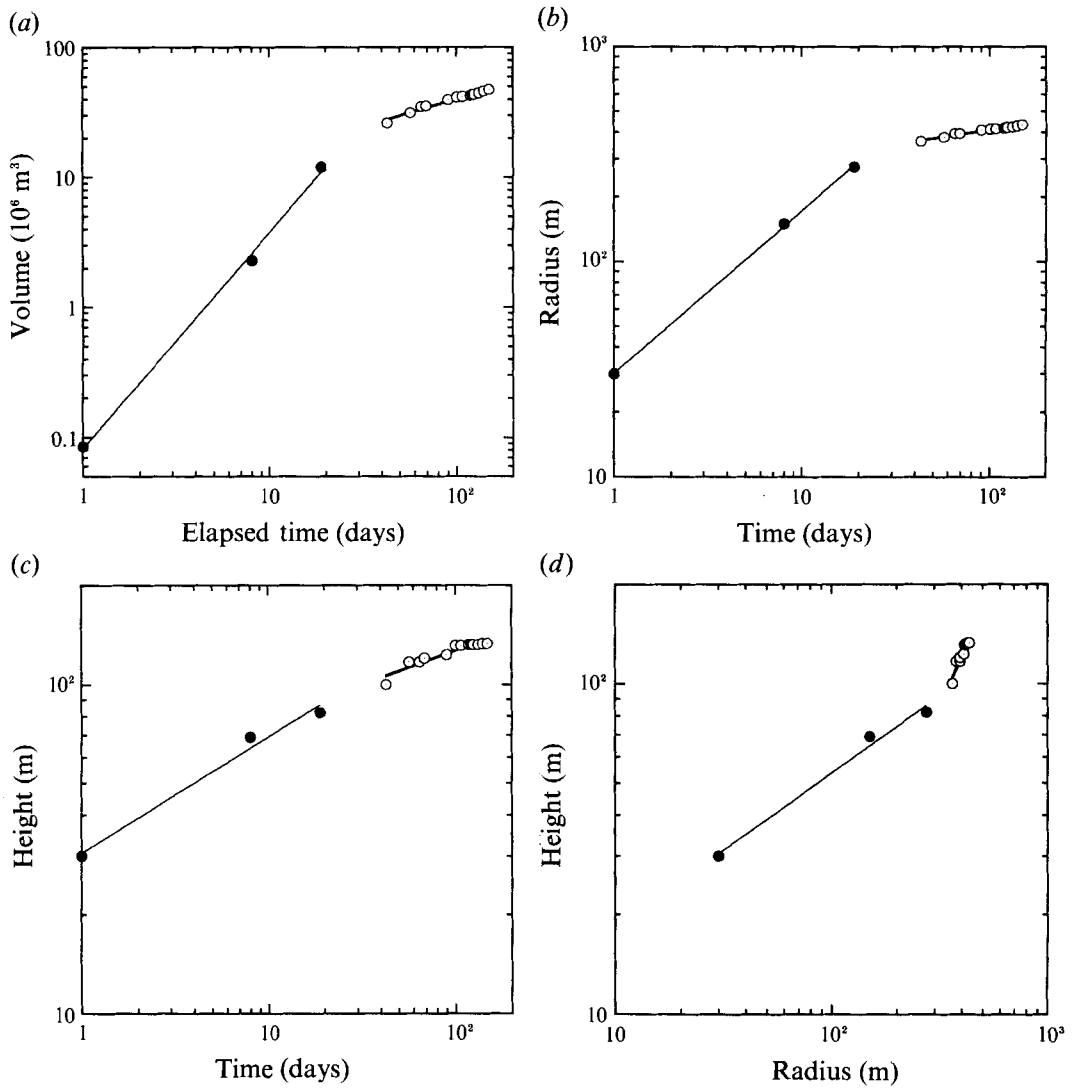

FIGURE 10. Data for the growth of the lava dome that appeared at Soufrière of St Vincent between 7 May and 2 October 1979. The increase of dome volume (*a*) is not adequately fitted by a single power law but is well described by two power law curves (21), as discussed in the text. Also plotted are (*b*) the evolution of dome radius, (*c*) height as a function of time and (*d*) height as a function of radius (*d*). The break between two power laws fits ((22) and (23)) at 20–40 days does not necessarily imply a change of dynamical regime for spreading, or even a significant change in the magma effusion rate, at that time. It simply allows a good approximation to the growth in terms of simple power laws. Data are taken from Huppert *et al.* (1982).

greater than $R/30$, or approximately 3 m at day 10. This is greater than, but comparable to, the thermal boundary-layer thickness scale of 1.3 m (and the thickness of solid) which should develop in that time. Thus, again, both yield strengths were probably of importance during this early stage of the extrusion. In both models the strength estimate confirms that the observed dome height of 30 m at day 1 of the record is greater than the height expected at transition from overpressure to buoyancy-driven flow (from (14*b*) $H^* \sim 3$ m and from (14 *d*) $H^* \sim 10$ m). Note also that the aspect

ratio at day 1 was $H/R \approx 1.0$, whereas by day 19 it had decreased to $H/R \approx 0.37$. Thus overpressure was probably significant at day 1, but all the evidence indicates that buoyancy subsequently become dominant.

For the second stage of growth of the Soufrière dome ($40 < t < 150$ days) the radius and height (figure 9*b–d*) are well described by

$$R \sim 49t^{0.13}, \quad H \sim 4.8t^{0.21}, \quad H \sim 0.013R^{1.5}. \tag{23}$$

For this period we compare the various models of table 1 using $\alpha = 0.44$ (table 3). Both viscous models again clearly fail because they predict decreasing dome height and a radius increasing too rapidly. This time the homogeneous plastic model fails also as the height is predicted to increase too slowly ($H \sim t^{0.087} \sim R^{0.5}$). Balances of either overpressure or buoyancy with crust yield strength provide adequate fits to the data. However, it was concluded that overpressure was replaced as the dominant driving force by buoyancy during the early stage of growth. Hence overpressure is unlikely to become dominant in later stages (although it cannot be ruled out when $\alpha < \frac{3}{4}$). The dome aspect ratio of ~ 0.3 also indicates that buoyancy continues to be important. Hence we conclude that this second stage of growth is best described by the buoyancy–crust strength model. From this model we predict $R \sim t^{0.094}$, $H \sim t^{0.25}$ and $H \sim R^{2.67}$. Here the power for $H(R)$ is larger than the value (1.5) deduced from the data. However, the predicted form of $H(R)$ is sensitive to α because α is small ($\alpha = 0.58$ gives the 'observed' power), and the uncertainty in the 'observed' power is as large as 20%.

If a buoyancy–crust strength balance is assumed to hold for the second stage of growth of the Soufrière dome, the best fit of the $H \sim t^{\frac{1}{4}}$ law (table 1) to the height data at $t > 40$ days implies an effective yield strength $\sigma_c \sim 1.5 \times 10^8$ Pa. This strength is identical to that found above for the Mount St Helens dome. The similarity is perhaps surprising given the large difference in the duration of the extrusions, the episodic nature of the magma extrusion at Mount St Helens and the different lava compositions. On the other hand, it may reflect the maximum yield strength achieved by a fractured, jumbled carapace of solidified lava near the ambient temperature on domes of this size, and may not depend on the precise lava composition or thickness of solid. Possible explanations for the relatively small strength obtained for the first 20 days of growth are a higher temperature for most of the solid carapace at small times, a dependence of effective strength on crust thickness while the crust is relatively thin (because deformation of the crust is then more two-dimensional), or a strain-rate dependence of the effective strength. Whatever the explanation for the similar crustal strengths on the two domes, the above results provide evidence that growth of lava domes is controlled by the strength of their surface crust rather than by the viscosity or yield strength of the lava in their interior.

7.3. *Morphology of natural and analog domes*

Having determined the dynamical regimes for the two lava domes and the wax experiments, we note a broader consistency between their observed morphologies and estimated values of the dimensionless rate of crust development (Ψ). For the lava domes the data indicate that crust strength provides the dominant retarding force over most of the observation period, and our estimates given Ψ of order one. These characteristics are consistent with those found for the wax analog, where the radius and height indicate flow controlled by the strength of the solidified crust at $\Psi < 10$. The only discrepancy is that the wax in experiments at $\Psi < 3$ formed flows made up of many small lobes or pillows (similar in appearance to slow submarine extrusions of

basaltic melt), whereas the lava domes appear to be made up of only a small number of lobes. Thus the similarity between the wax flows and lava domes is complete if the domes are identified as one or more large 'pillows' several hundred times larger than a typical submarine pillow, or if the domes are viewed as 'rifting' sheet flows. In the first of these views sub-aerial extrusions of very viscous andesite and dacite melts are required to form 'pillows' much larger than those formed by submarine eruptions of low-viscosity melts. At this stage we can only conjecture that the size of 'pillows' formed by a given extrusion may be related to the value of Ψ, which is possibly an order of magnitude smaller for submarine eruptions than for the lava domes (Griffiths & Fink 1992*b*). On the other hand, the 'rifting' regime is indicated by the observation of linear crease structures (Anderson & Fink 1992), somewhat like 'rifts' in the wax experiments, on the Mount St Helens dome (see figure 8). Furthermore, the estimated Ψ values for the lava domes, which have large uncertainties, place them near the edge of the range of conditions giving 'pillow' morphology, hence transitional with conditions giving 'rifting'. The value of Ψ for Mount St Helens would be significantly larger and well within the 'rifting' regime if it were based on the instantaneous effusion rate during each enlargement episode rather than on the time-averaged rate.

For the Soufrière dome we have concluded that the yield strength of the interior magma could have exercised a significant influence on the lateral spreading during the first days of eruption, but that crust strength became dominant within the first 20 days. Additional evidence for such a transition is available from the growth of a lobe on top of the St Helens dome in October 1986. A time lapse movie provides us with the length and width of this lobe, which grew from a linear spreading centre and spread almost two-dimensionally over a period of 160 minutes. Power laws fit the data extremely well, giving the length as $L = 0.627t^{0.769}$ and the height as $H = 1.43t^{0.460}$. Taking into account the shape of the lobe we estimate that the volume increased as

$$V \approx 0.75LH \sim qt^{\alpha},$$

where $q \approx 0.673$ and $\alpha \approx 1.2$. Comparison with the model predictions for line sources (table 1) shows that for this value of α the best fit to the observations is given by a balance of homogeneous yield strength and buoyancy: $L \sim t^{0.80}$, $H \sim t^{0.40}$. The other models, including that with a dominant crust strength, are not satisfactory. Fitting the predicted form for $H(t)$ to the data and using the above values of q and α we estimate the interior shear strength to be $\sigma \sim 1.1 \times 10^5$ Pa, a value comparable to that found for the interior of the Soufrière dome in its early stages. This illustrates the point that extrusions can be dominated by either interior or crustal stresses, depending on effusion rate and time available for development of the crust.

8. Conclusions

Scaling analyses for the lateral flow of material with a temperature-dependent rheology show that a number of different dynamical regimes involving buoyancy, overpressure, shear strength and tensile strength are possible in the presence of surface cooling. Under many conditions the shear stress applied to a plastic or brittle crust, which must be deformed because it comes in contact with the base at the flow front, provides the dominant retarding force controlling lateral spreading of the flow. Our laboratory experiments with wax spreading and solidifying beneath cold water show some of these dynamical regimes. In cases where the cooling is very slow or the effusion rate large solid crust does not form until the flow front is a large distance from the source. In these cases there exists a viscous–buoyancy balance previously discussed by

Huppert (1982) in the context of uniform isothermal gravity currents. In general, however, our wax flows, like lavas, are thermally and rheologically heterogeneous. This is particularly so once the surface begins to solidify. The wax flows then become dominated by the yield strength of the thin crust, which balances the buoyancy force. At very rapid cooling rates or small effusion rates there is another regime in which the dynamical balance is between overpressure and tensile strength of the crust. If the effusion rate does not decline too rapidly, the latter flows eventually enter the buoyancy-driven regime. The relative importance of shear and tensile strengths in the crust is not always clear when buoyancy is the dominant driving force. However, we expect tensile strength to dominate small 'overpressurized' domes or lobes (as suggested by Iverson 1990) but an effective shearing strength to dominate large domes and flatter, faster spreading flows in which shear stresses are important and on which the crust is fragmented or deformable.

The dynamical regimes appear to be identified with different styles of flow morphology. In the wax experiments a viscous–buoyancy balance is associated only with flows on which there is little or no solid crust ($\Psi > 80$), a buoyancy–crust strength balance is associated with sheets of solid crust on the surface, where differential motion is accommodated either at rifts or by surface buckling (intermediate Ψ), and the overpressure–tensile strength regime occurs at early stages of extrusions under rapid cooling conditions ($\Psi < 3$), where a strong brittle crust forms over bulbous 'pillow'-like outgrowths. If this correspondence carries over to lava flows, the observed morphology of lavas might be used as an indicator of the dynamics of flow emplacement.

The scaling analyses predict that the rheology of the complex crustal layer is the dominant factor in resisting advance of the flow front when the ratio of crust thickness (near the flow front) to flow length is greater than the ratio of the crust's yield stress to the basal shear stress exerted on the bulk of the flow (10). Hence, if the effective yield strength σ_c of a solid carapace is several orders of magnitude greater than the shear strength σ of the interior magma (we have found $\sigma_c \sim 10^8$ Pa and $\sigma \sim 10^5$ Pa for two lava domes), flows with small and moderate values of Ψ will be governed by the crust strength once the crust develops a thickness several orders of magnitude less than the flow length. Thus a 10 m thick carapace over a dome 1 km in radius is likely to be sufficient to control the spreading of the lava. Data for the Mount St Helens and Soufrière lava domes support the hypothesis that the shape and rate of spreading of these domes is controlled by crust strength and not by stresses in the interior magma. The results should also be relevant to smaller outbreaks from lava flows, such as submarine basalt 'pillows' or sub-aerial pahoehoe 'toes'.

We thank Derek Corrigan and Tony Beasley for construction of equipment and assistance with the experiments, and Nathan Bridges for taking the experimental data from film. Research was supported by NASA Grant NAGW 529 from the Planetary Geology and Geophysics Program, National Science Foundation Grant EAR 9018216, and a Visiting Fellowship from The Australian National University.

REFERENCES

ANDERSON, S. W. & FINK, J. H. 1992 Crease structures: indicators of emplacement rates and surface stress regimes of lava flows. *Geol. Soc. Am. Bull.* **104**, 615–625.

BLAKE, S. 1990 Viscoplastic models of lava domes. In *Lava Flows and Domes: Emplacement Mechanisms and Hazard Implications* (ed. J. H. Fink), IAVCEI Proc. in Volcanology, vol. 2, pp. 88–128.

CRISP, J. A. & BALOGA, S. M. 1990 A model for lava flows with two thermal components. *J. Geophys. Res.* **95**, 1255–1270.

DENLINGER, R. P. 1990 A model for dome eruptions at Mount St Helens, Washington based on subcritical crack growth. In *Lava Flows and Domes: Emplacement Mechanisms and Hazard Implications* (ed. J. H. Fink), IAVCEI Proc. in Volcanology, vol. 2, pp. 70–87.

DIDDEN, N. & MAXWORTHY, T. 1982 The viscous spreading of plane and axisymmetric gravity currents. *J. Fluid Mech.* **121**, 27–42.

FINK, J. H. & FLETCHER, R. C. 1978 Ropy pahoehoe: Surface folding of a viscous fluid. *J. Volcanol. Geotherm. Res.* **4**, 151–170.

FINK, J. H. & GRIFFITHS, R. W. 1990 Radial spreading of viscous–gravity currents with solidifying crust. *J. Fluid. Mech.* **221**, 485–510.

FINK, J. H. & GRIFFITHS, R. W. 1992 A laboratory analog study of the morphology of lava flows extruded from point and line sources. *J. Volcanol. Geotherm. Res.* **54**, 19–32.

FINK, J. H., MALIN, M. C. & ANDERSON, S. W. 1990 Intrusive and extrusive growth of the Mount St Helens lava dome. *Nature* **348**, 435–437.

GRIFFITHS, R. W. & FINK, J. H. 1992*a* The morphology of lava flows under planetary environments: predictions from analog experiments. *J. Geophys. Res.* **97**, 19739–19748.

GRIFFITHS, R. W. & FINK, J. H. 1992*b* Solidification and morphology of submarine lavas: a dependence on extrusion rate. *J. Geophys. Res.* **97**, 19729–19737.

HULME, G. 1974 The interpretation of lava flow morphology. *Geophys. J. R. Astron. Soc.* **39**, 361–383.

HUPPERT, H. E. 1982 The propagation of two-dimensional and axisymmetric viscous gravity currents over a rigid horizontal surface. *J. Fluid Mech.* **121**, 43–58.

HUPPERT, H. E., SHEPHERD, J. B., SIGURDSSON, H. & SPARKS, R. S. J. 1982 On lava dome growth, with application to the 1979 lava extrusion of the Soufrière of St Vincent. *J. Volcanol. Geotherm. Res.* **14**, 199–222.

IVERSON, R. M. 1990 Lava domes modelled as brittle shells that enclose pressurised magma, with application to Mount St Helens. In *Lava Flows and Domes: Emplacement Mechanisms and Hazard Implications* (ed. J. H. Fink), IAVCEI Proc. in Volcanology, vol. 2, pp. 47–69.

KILBURN, C. R. J. & LOPES, R. M. C. 1991 General patterns of flow field growth: Aa and blocky lavas. *J. Geophys. Research* **96**, 19721–19732.

LISTER, J. R. & KERR, R. C. 1989 The propagation of two-dimensional and axisymmetric viscous gravity currents at a fluid interface. *J. Fluid Mech.* **203**, 215–249.

MCBIRNEY, A. R. & MURASE, T. 1984 Rheological properties of magmas. *Ann. Rev. Earth Planet. Sci.* **12**, 337–357.

PINKERTON, H. 1987 Factors affecting the morphology of lava flows. *Endeavour* **11**, 73–79.

PINKERTON, H. & SPARKS, R. S. J. 1976 The 1975 sub-terminal lavas, Mount Etna: A case history of the formation of a compound lava field. *J. Volcanol. Geotherm. Res.* **1**, 167–182.

SHAW, H. R. 1969 Rheology of basalt in the melting range. *J. Petrology*, **10**, 510–535.

SHAW, H. R. & SWANSON, D. A. 1970 Eruption and flow rates of flood basalts. *Proc. Second Columbia River Basalt Symposium*, pp. 271–299. Eastern Washington State College Press.

SWANSON, D. A. & HOLCOMB, R. T. 1990 Regularities in growth of the Mount St Helens dacite dome, 1980–1986. In *Lava Flows and Domes: Emplacement Mechanisms and Hazard Implications* (ed. J. H. Fink), IAVCEI Proceedings in Volcanology, vol. 2, pp. 1–24.

WALKER, G. P. L. 1972 Compound and simple lava flows and flood basalts. *Bull. Volcanol.* **35**, 579–590.

WALKER, G. P. L. 1973 Lengths of lava flows. *Phil. Trans. R. Soc. Lond.* A **274**, 107–118.

WILSON, L. & HEAD, J. W. 1983 A comparison of volcanic eruption processes on Earth, Moon, Mars, Io and Venus. *Nature* **302**, 663–669.